Biosynthesis of Silver, Titanium Dioxide and Silver-Titanium Dioxide Composite Nanoparticles Mediated by Bacillus Amyloliquefaciens PGB240 and its Biological Applications

Gowthami M.[1]; Sindhushri Chauhan[2]; Shivakantkumar Adhikari[3*]

[1]Centre for Research and Innovations, Adichunchanagiri University, Mandya, Karnataka- 571448, India
[2]Department of Studies and Research in Biotechnology and Microbiology, Jnanasiri Campus, Tumkur University, Tumakuru. Bidarakatte- 572 118, India
[3]Department of Studies and Research in Biotechnology and Microbiology, Jnanasiri Campus, Tumkur University, Tumakuru. Bidarakatte- 572 118, India

Correspondence Author: Shivakantkumar Adhikari[3*]

Publication Date: 2026/09/03

Abstract: *Bacillus amyloliquefaciens* is a Gram-positive, spore-forming bacterium found in soil, plants, water, and food, known for promoting plant growth by fixing nitrogen, solubilizing phosphate, and producing antimicrobial compounds. In this study, *Bacillus amyloliquefaciens PGB240* was used to synthesize silver (Ag), titanium dioxide (TiO_2), and silver-titanium dioxide (Ag-TiO_2) nanoparticles (NPs). Their physicochemical properties were analyzed using UV-Vis, XRD, EDX, SEM, FTIR, and DLS techniques. Antibacterial activity was tested against *Streptococcus pyogenes, Staphylococcus aureus, Streptococcus pneumoniae,* and *Escherichia coli,* with all NPs showing significant inhibition. Antioxidant assays revealed strong free radical scavenging activity: 96.7% (Ag), 97.9% (TiO_2), and 95.9% (Ag-TiO_2). Phytotoxicity tests on maize and cucumber seeds showed enhanced germination rates compared to untreated seeds. Maize achieved 100% germination with all NPs, while cucumber showed 100% with Ag, and 80% with TiO_2 and Ag-TiO_2. Root growth was also promoted, with maximum lengths of 2.88 cm (Ag, 0.5 mg/mL), 1.58 cm (TiO_2, 1.5 mg/mL), and 2.94 cm (Ag-TiO_2, 1.0 mg/mL). These findings highlight their potential in agriculture and biomedicine.

Keywords: *Biosynthesized Nanoparticles, Antibacterial Properties, Antioxidant Activities, Seed Germinations, DPPH Free Radicals, X-ray Diffraction, Dynamic Light Scattering*

How to Cite: Gowthami M.; Sindhushri Chauhan; Shivakantkumar Adhikari (2026) Biosynthesis of Silver, Titanium Dioxide and Silver-Titanium Dioxide Composite Nanoparticles Mediated by Bacillus Amyloliquefaciens PGB240 and its Biological Applications. *International Journal of Innovative Science and Research Technology*, 11(8), 2562-2579. https://doi.org/10.38124/ijisrt/26aug1001

I. INTRODUCTION

Bacillus amyloliquefaciens, classified within the super kingdom bacteria, belongs to the family *Bacillaceae* and the genus *Bacillus*. It is a gram-positive, rod-shaped, endospore-forming bacterium exhibiting a chain-forming cellular morphology. In 1943, *B. amyloliquefaciens* was first isolated, and until the 1980s, it was considered to be *Bacillus subtilis.* This species is universally distributed across diverse environmental niches, including plants, foods, soil, and aquatic ecosystems. According to the global microbial inventory, 273 distinct strains of *B. amyloliquefaciens* have been isolated from several sources. Despite the heterogeneity among strains regarding physiological traits and biotechnological applications, *B. amyloliquefaciens* is broadly recognized as a non-toxic and biosafe microorganism. Its capacity to form robust endospores enables it to endure harsh environmental circumstances, contributing to its ecological versatility (1).

This robustness supports its utility across various sectors: in food science for enzyme production, probiotic and prebiotic formulation, and development of functional and bioactive foods; in pharmaceuticals for anticancer, antimicrobial, and antidiabetic agents; in agriculture for prevention of plant and animal diseases; and in environmental biotechnology, for applications such as waste treatment and biofuel production (2). The primary and secondary metabolites produced by *B. amyloliquefaciens* hold significant potential for novel food and medical applications. These include microbial exopolysaccharides with demonstrated antitumor, antiviral, immunomodulatory, and antioxidant properties, and anticancer effects (3). Furthermore, secondary metabolites such as lipopeptides, specifically surfactin, serrawettin and viscosin, exhibit multifunctional bioactivities, including antimicrobial, antiviral, anti-inflammatory, and antiadhesive effects. Overall, beyond its established roles in food and pharmaceutical industries, *B. amyloliquefaciens* is extensively applied in fermentation, biosynthesis, and hydrolytic processes (4).

Nanoparticles, typically ranging from 1 to 100 nanometers, are incorporated into materials like metals, semiconductors, and polymers, exhibiting unique chemical and physical properties. Because of these properties, nanoparticles are extremely beneficial in electronics, health, and environmental protection (5). Nanotechnology, particularly the biosynthesis and application of nanomaterials, is rapidly growing, with significant potential across various fields. Silver nanoparticles (Ag NPs), titanium dioxide nanoparticles (TiO_2 NPs), and Ag-TiO_2 composites are commonly used in therapy, biomolecular detection, catalysis, and as antimicrobial agents. Compared to traditional techniques, microbial synthesis of nanoparticles is more environmentally friendly, as it uses less hazardous chemicals and can function in milder environments (6). This study focuses on using *Bacillus amyloliquefaciens* for the biosynthesis of these nanoparticles, offering an eco-friendly alternative to chemical and physical synthesis methods (7).

Bacillus amyloliquefaciens PGB240 is an aerobic, Gram-positive, spore-forming bacterium generally found in soil. Due to its production of highly efficient proteins, it is widely utilized in industrial processes for the production of enzymes, chemicals, and antimicrobial agents. This bacterium synthesizes several enzymes, including α-amylase, xylanases, lichenase, lipase, cellulase, and pectinase, which play a role in the biosynthesis of nanoparticles (NPs) (8).

Numerous applications have demonstrated the utilization of TiO_2 nanoparticles produced by this bacterium for antibacterial activity and photocatalytic degradation of different cationic and anionic dyes. Additionally, it has been revealed that when exposed to visible light, these biosynthesized TiO_2 NPs have antimicrobial properties (9, 10, 11).

For the purposes of this study, synthesizing NPs using *Bacillus amyloliquefaciens* PGB240 represents an environmentally friendly approach to reducing environmental risks while making useful materials applicable in multiple fields. The present investigation focuses on employing *Bacillus amyloliquefaciens* PGB240 extracts to sustainably biosynthesize silver (Ag NPs), titanium dioxide (TiO_2 NPs), and silver-titanium dioxide (Ag-TiO_2 NPs) composite nanoparticles. Several analytical methods, such as UV-Vis spectroscopy, scanning electron microscopy (SEM), transmission electron microscopy (TEM), dynamic light scattering (DLS), X-ray diffraction (XRD), and Fourier transform infrared spectroscopy (FTIR), were used to characterize these biosynthesized NPs. Furthermore, the antimicrobial, antioxidant, and seed germination activities of Ag NPs, TiO_2 NPs, and Ag-TiO_2 composite NPs were evaluated (12).

II. METHODOLOGY

A. Isolation of Bacterial Strain from Goat Milk and Maintenance of Bacterial Cultures

The Bidri breed goat's milk was used to isolate the bacterial strain. 16S rRNA-based barcoding was used to identify the isolated bacteria, and the barcoding sequence was then submitted to GenBank. The strain was incubated for 24 hours at 37 ± 2°C on Nutrient Agar (NA) medium. It was preserved on slants containing 10 ml of Nutrient Agar, while pure cultures of the isolates were regularly subcultured and maintained for further studies. This strain's nanoparticles were optimally biosynthesized in nutrient broth (pH 7.0). Bacillus sp. was cultivated in a 50 ml nutrient broth flask and a 100 ml nutrient broth. *Bacillus amyloliquefaciens* strain PGB240 was treated following the same protocol, with all inoculated conical flasks incubated on an orbital shaker at 120 rpm for 24 hours (13).

B. Extracellular Synthesis of Nanoparticles

Bacillus amyloliquefaciens was inoculated into 100 mL of sterilized LB broth to investigate the synthesis of silver, titanium dioxide, and silver titanium dioxide composite nanoparticles (14). The conical flasks were incubated at 28°C on an orbital shaker at 180 rpm for 24 hours. Following incubation, the culture was centrifuged using an Eppendorf centrifuge for 10 minutes at 12,000 rpm to separate the biomass from the supernatant. Silver and titanium dioxide nanoparticles were extracellularly biosynthesized using the isolated supernatant (15). Nanoparticle biosynthesis involved 115 mL of an aqueous solution of 3 mM ($AgNO_3$/TiO_2); the final concentration was treated with 35 mL of culture supernatant solution in a conical flask at 200 rpm at 37° C for 48 hours and maintained in the dark. The experimental culture supernatant without the addition of $_{AgNO3}$/TiO_2 was maintained as a control. After 48 hours, the solution was centrifuged, and the subsequent pellet was rinsed with ethanol, dried at 70°C for 15 hours, and ground into a fine powder (13).

C. Preparation of Ag/TiO_2 Composite Nanoparticle

50 mL of ethanol-water solution was used to dissolve 2.0 mM Ti (SO4)2. After 10 minutes of magnetic stirring, various concentrations of AgNO3 and NaOH (0. 25 mM, 0. 50 mM, 1 mM, and 2 mM) were gradually added to the aforementioned solution. The resulting mixture was transferred to a 100 mL Teflon-lined autoclave, which was then filled with deionized water up to 85% of its total volume. The autoclave was sealed, heated to 160°C for six hours, and then allowed to naturally cool to ambient temperature. The final products were obtained by Eppendorf centrifugation at 15,000 rpm, repetitively cleaned with ethanol and distilled water, and then vacuum-dried (16).

D. Characterization of Silver, Titanium Dioxide and Silver-Titanium Dioxide Composite Nanoparticles

➢ *UV–Visible Spectrum*

The absorbance peak of the biosynthesized Ag, TiO_2, and Ag-TiO_2 composite NPs was determined through UV-Vis measurements conducted with a UV-Vis spectrophotometer (Agilent, Cary 60, United States). The analysis was conducted over a wavelength range of 200 to 800 nm, with a resolution of 1 nm. The UV-Vis analysis was conducted using well-dispersed Ag, TiO_2, and Ag-TiO_2 composite NPs. A 2 mL aliquot was subsequently transferred into a quartz cuvette, and the absorbance at 400 nm was measured using the UV-Vis spectrophotometer (9).

➢ *Scanning Electron Microscopy-Energy Dispersive X-ray Spectroscopy (SEM-EDX) Analysis*

The surface morphology of Ag, TiO2, and Ag-TiO2 composite NPs was analyzed by SEM (JEOL, Tokyo, Japan) and energy-dispersive X-ray spectroscopy (EDX). A small amount of Ag, TiO_2, and Ag/TiO_2 composite NPs was applied to carbon tape using a fine brush. Scanning electron microscopy (SEM) was employed to capture the micrographs, and elemental composition was examined using energy-dispersive X-ray spectroscopy (EDS) with a JEOL JEM-2010 detector integrated into the SEM system (17).

➢ *Dynamic Light Scattering (DLS) Analysis*

Dynamic light scattering was used to analyze the size of Ag, TiO_2, and Ag-TiO_2 composite nanoparticles (DLS with a Zetasizer Nano ZN from Malvern Panalytical Ltd., Worcester, UK). Zeta potential measurements were conducted at 25 °C using dynamic light scattering (DLS) to evaluate the surface charge distribution of the nanoparticles (12).

➢ *Fourier Transform Infrared (FT-IR) Analysis*

Fourier Transform Infrared (FT-IR) spectroscopy was employed to identify the various functional groups present in the biosynthesized silver (Ag), titanium dioxide (TiO_2), and silver-titanium dioxide (Ag-TiO_2) composite nanoparticles. The investigation was executed using a PerkinElmer SP 6500 spectrometer (New York City, United States) with a spectral resolution of 1 cm^{-1}, spanning the range of 400 to 4000 cm^{-1}. The samples of silver (Ag) nanoparticles, titanium dioxide (TiO_2) nanoparticles, and the Ag-TiO_2 composite were finely ground and mixed with spectroscopic-grade potassium bromide (KBr) in a 1:100 ratio by weight. All spectra were documented at room temperature, and background corrections were performed using a blank KBr pellet (18).

➢ *X-ray Diffraction Analysis*

X-ray diffraction (XRD) analysis was performed to determine the crystalline phases and structural characteristics of the synthesized silver (Ag), titanium dioxide (TiO_2), and silver-titanium dioxide (Ag-TiO_2) composite nanoparticles. 25 mg of Ag, TiO_2, and Ag- TiO_2 composite NPs were individually positioned on a sample holder and subsequently examined using a Rigaku Mini Flex 300/600 X-Ray Diffractometer instrument (Japan) with Cu Kα radiation (λ = 1.5406 Å), operated at 45 kV and a current of 20 mA. Data were collected over a 2θ range of 20-80° with a step size of 0.02°. The obtained diffraction patterns were examined using standard reference patterns from the Joint Committee on Powder Diffraction Standards (JCPDS) database to identify the crystalline phases (13).

E. Antimicrobial Assay

The antibacterial assay of biosynthesized Ag, TiO_2, and Ag-TiO_2 nanoparticles was evaluated against gram-positive bacteria (*Staphylococcus aureus, Streptococcus pneumoniae* and *Streptococcus pyogenes*) and a gram-negative bacterium (*Escherichia coli*) using the agar well diffusion assay, following the method described by (19). The microbial strains were cultured until a turbidity level of 0.5 according to the McFarl and standard. Under aseptic conditions, the bacterial cultures were consistently spread onto nutrient agar plates using a sterile cotton swab. Under aseptic conditions, wells measuring 6 mm in diameter were punched into the agar plates using a sterile cork borer. Approximately 100 µL of biosynthesized Ag, TiO_2, and Ag-TiO_2 composite nanoparticles (NPs) at concentrations of 1 mg/mL and 5 mg/mL were added to each well. Rifampicin served as the positive control, while double distilled water was used as the negative control. Subsequently, the inoculated plates were incubated at 37 °C for 24 hours. Following incubation, the diameter of the inhibition zones was measured in millimeters (mm) to assess antibacterial activity. The The diameter of the inhibitory zone was determined in millimeters (mm) following the incubation time (20).

F. Antioxidant Assay

➢ *Superoxide ($O2^-$) Radical Scavenging Activity*

This activity of Ag, TiO_2 and Ag-TiO_2 composite NPs was performed according to Keshari et al. (21). Superoxide radicals were produced through the process of oxidation and subsequently analyzed via reduction of Nitro blue tetrazolium (NBT). A reaction mixture was containing 0.2 mL of nanoparticles (NPs) at veriying ranging from 100 to 500 µg/mL in methanol, 1 mL of 16 mM Tris–HCl buffer (pH 8), and 1 mL of 50 µM nitro blue tetrazolium (NBT) solution, followed by incubation at 25 °C for 5 minutes, after which the OD was taken at 560 nm using a UV–Vis spectrophotometer. Vitamin C was used as standard and prepared same as Ag, TiO_2 and Ag-TiO_2 NPs. The superoxide inhibition (%) was calculated by the formula:

$$\text{Inhibition (\%)} \quad \frac{Sc\text{-}Ss}{Ss} \times 100$$

Where, Sc is the absorbance of control (all the reagent except the test sample) while Ss is the absorption of NPs/vitamin C.

➢ *2, 2-Diphenyl-1-Picrylhydrazyl (DPPH) Activity*

The 2, 2-diphenyl-1-picrylhydrazyl (DPPH) was carried out according to Keshari et al. (21). The assessment of the free radical scavenging activity of Ag, TiO_2 and Ag-TiO_2NPs and standard vitamin C was conducted using the constant radical DPPH. A volume of 1ml from several concentrations of Ag, TiO_2 and Ag-TiO_2 NPs (25, 50, 75 and 100µg/ml) was

ISSN No:-2456-2165 https://doi.org/10.38124/ijisrt/26aug1001

mixed with 1ml of a freshly prepared DPPH solution (1mM in methanol) and subjected to thorough vortex mixer. The reaction mixture was incubated at room temperature in the dark for 30 minutes to facilitate stable radical interaction. The absorbance was then measured at 517 nm using a UV–Vis spectrophotometer (Systronics, AU-2701) to assess the DPPH radical scavenging activity of the nanoparticles. Methanol served as the blank, while a control solution containing DPPH and all other reagents except the nanoparticle samples were used for comparison. The following formula was used to determine the DPPH radical scavenging activity percentage.

Where A control is the optical density of the control reaction (Ascorbic acid is used as control) and A sample is the absorbance in the presence of the nanoparticle sample.

G. Seed Germination Test

To study the effects of nanoparticles on seed germination, different concentrations of silver nanoparticles (Ag NPs), titanium dioxide nanoparticles (TiO_2 NPs), and silver-titanium dioxide composite nanoparticles (Ag-TiO_2 Composite NPs) were prepared. Seeds from two various plants were subjected to these nanoparticles at increasing concentrations of 0.05, 0.1, 0.5, 1, 1.5, 2, and 2.5 mg/mL. Seeds treated with double-distilled water served as the control group.

- *Seed Germination*

Maize and cucumber seeds were soaked in a 5% sodium hypochlorite solution for a 10 min to achieve surface sterility. Subsequently, they were immersed in double-distilled water for 10 min, followed by three rinses with distilled water. Finally, the seeds were immersed in a series of prepared nanoparticle suspensions (Ag, TiO_2, Ag-TiO_2 Composite NPs) for approximately 24hours (22). Blotting paper was placed in a 100 × 15 mm Petri dish, followed by the addition of 5 mL of test solution from each treatment. Seeds that were exclusively treated with deionized water consider as the control. After the treatments, ten seeds were arranged with a one-centimetre gap between them on each cotton pad. Each treatment repeated thrice. The Petri dishes were maintained in an incubator that provided 12hrs light and 12hrs dark cycle, at temperature of 25±2°C and maintained 60% relative humidity. The germinated seeds were monitored and counted daily, focusing on the emergence of a 2mm radicle, for up to 7 days. The rates of seed germination and the mean germination time were determined, while the lengths of both the seedling shoots and roots were assessed (20, 23).

- *Seed Germination Measurement*

The final seed germination % was determined by enumeration the total number of seeds that successfully germinated at the completion of the experiment. All experiments were carried out following the International Rules for Seed Testing (24). Additional germination parameters were calculated using the standard equations established by (25).

Germination Percentage (GP %) = (Gf/n) × 100

Where Gf represents the total number of seeds that germinated by the experiment's conclusion, while n signifies the total number of seeds initially used in the test.

Mean Germination Time (MGT) = Σ NiDi/n

Where Ni represents the cumulative number of seeds that have germinated up to the ith day, while Di signifies the number of days elapsed from the experiment's initiation until the ith counting. Additionally, n denotes the total number of seeds that germinated throughout the entire experiment (26).

Germination Rate (GR) = Σ Ni/ΣTiNi

Where Ni is the number of newly germinated seeds at time Ti.

GR = (a/1) + (b-a/2) + (c-b/3) +.....+ (n-n-1/N)

H. Statistical Analysis

Measurements from three triplicates encompassing each treatment and its corresponding controls, were used to calculate the means and standard deviations.

III. RESULTS AND DISCUSSION

A. Isolation Bacteria Strain from Bidri Breed Goat Milk Sample

The bacterial isolate obtained from a goat sample was molecularly identified as *Bacillus amyloliquefaciens* strain PGBE240 via 16S rRNA gene sequencing, with the sequence deposited in GenBank under accession number OP315026. The biosynthesized silver nanoparticles (Ag NPs), titanium dioxide nanoparticles (TiO_2 NPs), and their silver-titanium dioxide composite (Ag-TiO_2 composite NPs) demonstrated potent and broad-spectrum antibacterial efficacy against multiple gram-positive and gram-negative pathogenic strains. Moreover, Ag NPs, TiO_2 NPs, and Ag-TiO_2 composite NPs showed significant potential as antibacterial agents against multidrug-resistant bacteria (27). Investigating the dose-response effects of silver nanoparticles (Ag NPs), titanium dioxide nanoparticles (TiO_2 NPs), and Ag-TiO_2 composite nanoparticles on plants is key for improving their application in agriculture. Such optimization can enhance crop productivity and bolster plant resistance to pathogens. Moreover, utilizing nanoparticles at carefully controlled concentrations may mitigate potential environmental risks linked to their accumulation (28, 22). The plant response to these nanoparticles is dose-dependent, where specific concentrations encourage development more successfully than controls, while excessively low or high doses are harmful. Numerous reports recommended that appropriate concentrations of Ag NPs, TiO_2 NPs, and Ag-TiO_2 composite NPs are crucial for improving seed germination, enhancing chlorophyll content and photosynthetic efficiency, and increasing the efficiency of fertilizer and water use (29).

B. Characteristics of Prepared Ag, TiO_2 and Ag-TiO_2 Composite Nanoparticles

To analyze the structure, size, morphology, chemical composition, and charge of the biosynthesized nanoparticles,

ISSN No:-2456-2165 https://doi.org/10.38124/ijisrt/26aug1001

several characterization methods were performed, including UV–Vis absorption spectroscopy (UV–Vis), dynamic light scattering (DLS), FT-IR, XRD, and SEM-EDS.

- *UV-Visible Spectroscopy Analysis*

UV-visible spectroscopy in the 200–500nm range was used to analyze silver nanoparticles (Ag NPs) and the 200–800nm range for titanium dioxide nanoparticles (TiO_2 NPs) (9). The UV-Vis spectra of Ag and TiO_2 NPs synthesized by *Bacillus amyloliquefaciens* showed peaks at 363nm and 293nm, respectively, indicating surface plasmon resonance (SPR). These peaks depend on factors like morphology, surface molecules, and contaminants. Ag-TiO_2 composite nanoparticles showed no peaks (Figure 1). Our results were in agreement with earlier work by Fouad et al. (30), who documented that *B. amyloliquefaciens* and *Bacillus subtilis* strains exposed to 3 mM silver nitrate ($AgNO_3$) effectively biosynthesized silver nanoparticles, as evidenced by a definite color change from light yellow to dark brown, indicative of nanoparticle formation. The presence and concentration of the biosynthesized Ag NPs was further validated through UV–visible spectrophotometric analysis, which exposed characteristic surface plasmon resonance peaks confirming nanoparticle synthesis. The absorption peaks appeared at 405 nm for *B. amyloliquefaciens* and 420 nm for *B. subtilis* following 24 hours of incubation and TiO_2 NPs biosynthesized from *Bacillus subtilis* MTCC 8322, which showed a peak near 394 nm (9). SPR peaks for Ag NPs shifted to higher wavelengths, correlating with a reduction in particle size compared to TiO_2 NPs. Factors such as agglomeration, surface charge, particle size, and shape affected the SPR of the Ag NPs (31). UV-Vis spectroscopy is a cost-effective method for nanoparticle characterization, measuring light intensity reflected from nanoparticles. Factors like shape, size, and concentration affect their optical properties. This technique evaluates light transmittance from 180 to 1100 nm, covering UV, visible, and near-infrared ranges, with absorption measured at specific wavelengths using the Beer-Lambert law (9, 32). Similarly, the UV–Vis spectroscopic analysis conducted by Jimoh et al. (27) revealed characteristic absorption peaks at approximately 414 nm for silver nanoparticles (Ag NPs) and 390 nm for titanium dioxide nanoparticles (TiO_2 NPs), indicating their successful synthesis and confirming their optical properties.

- *XRD Analysis*

The purity and crystalline structure of silver (Ag), titanium dioxide (TiO_2), and Ag-TiO_2 composite nanoparticles synthesized by *Bacillus amyloliquefaciens* were characterized using X-ray diffraction (XRD) analysis. The XRD patterns showed distinct peaks at specific 2θ angles, confirming the crystalline phases of the nanoparticles. The Ag nanoparticles displayed characteristic diffraction peaks at 38° (111), 46° (200), 55° (202), and 58° (220), consistent with a face-centered cubic (FCC) crystal structure. The most intense peak at 38° (111) confirmed their high degree of crystallinity. TiO_2 nanoparticles displayed peaks at 25º (101), 48º (200), 55º (211), 63º (204), and 77º (220), which align with the anatase phase TiO_2. The sharpness and intensity of these peaks suggest that the anatase phase was well-formed with good crystallinity. The XRD pattern of Ag-TiO_2 composite nanoparticles showed peaks from both Ag (FCC) and TiO_2 (anatase), indicating successful synthesis of the composite. The detection of diffraction peaks at specific angles, such as 25.3°, 37.8°, and 48.0°, indicates the coexistence of both Ag and TiO_2 phases within the composite nanoparticles, which may impart unique catalytic properties through synergistic interactions between the two materials (Figure 2). X-ray diffraction (XRD) was a widely employed technique for nanoparticle characterization, offering detailed information on phase composition, crystalline structure, grain size, and lattice parameters the latter of that may be estimated using the Scherrer equation. Similarly, (13). reported, applied to powdered samples, XRD involves generating X-rays by applying a voltage across electrodes, which emits X-rays upon impacting a metallic target. Previously, Titus et al. (33) investigated the crystalline structure and purity of silver nanoparticles synthesized by bacterial strains using X-ray diffraction (XRD). The diffraction pattern of silver nanoparticles biosynthesized by *Lactobacillus sp.* and *Bacillus sp.* revealed nine distinct peaks at 2θ values of 27.87°, 32.32°, 38.23°, 44.44°, 46.22°, 54.8°, 57.34°, 64.63°, and 77.39°. These peaks correspond to crystal planes (111), (200), (220), (222), and (311), confirming the formation of crystalline silver nanoparticles. Recently, Uthiravel, et al. (34) conducted X-ray diffraction (XRD) analysis to characterize green-synthesized TiO_2 and Ag-doped TiO_2 nanoparticles. The outcomes disclosed that TiO_2 showed sharp diffraction peaks corresponding to the anatase phase, indicating high crystallinity. Upon silver doping, additional peaks emerged in the XRD pattern, corresponding to the face-centered cubic (FCC) structure of metallic silver. Crystallite size calculations using the Scherrer equation showed an average size of 11.96 nm for pure TiO_2 and 41.8 nm for Ag-doped TiO_2. Similarly, Rathore et al. (35) reported the X-ray diffraction pattern of the synthesized TiO_2 nanoparticles, which exhibited characteristic peaks at 27.5° (110), 31.8° (121), 45.6° (210), 56.2° (211), 66.2° (204), and 75.4°. The peak observed at 27.5°, corresponding to the (110) crystal plane, along with the peak at 45.6° assigned to the (210) plane, confirms that the TiO_2 nanoparticles predominantly crystallize in the rutile phase. Awad et al. (36) presented the X-ray diffraction patterns of green-synthesized TiO_2 nanoparticles. The observed diffraction peaks correspond to 2θ values of 27.54° (101), 36.18° (103), 38.66° (004), 44.15° (200), 54.38° (105), 56.76° (211), 62.84° (204), 64.50° (213), 68.97° (116), and 70.42° (220), consistent with the standard crystallographic data (COD 9009086). These results confirm the successful synthesis of TiO_2 nanoparticles with a predominant anatase phase. Abd Elkodous et al. (37) investigated the XRD pattern of the P25 TiO_2 sample, identifying multiple diffraction peaks at 2θ values of 25.3°, 27.5°, 36.2°, 37.2°, 38.4°, 39.1°, 41.5°, 47.5°, 54.6°, 55.8°, 57.1°, 63.8°, 69.2°, 71.6°, 75.6°, and 76.7°. These peaks correspond to the (101), (110), (101), (103), (004), (112), (111), (200), (105), (211), (220), (204), (116), (220), (215), and (301) crystallographic planes, respectively. The pattern matches well with the reference data for both rutile (JCPDS No. 21-1276) and anatase (JCPDS No. 21-1272) phases of TiO_2, confirming the coexistence of these phases in the P25 sample.

ISSN No:-2456-2165 https://doi.org/10.38124/ijisrt/26aug1001

- *FTIR Analysis*

FTIR spectra of the biosynthesized silver (Ag), titanium dioxide (TiO_2), and Ag-TiO_2 composite nanoparticles revealed distinct functional groups involved in their formation and stabilization (Figure 3). Previously, Herrero et al. (38) described that Fourier Transform Infrared (FTIR) spectroscopy confirmed the presence of hydroxyl, alkene functional groups, and carbonyl which are known to contribute to the capping and stabilization of nanoparticles and Similar stabilization mechanisms of nanoparticles by bacterial biomolecules have been reported (39).

The Ag nanoparticles exhibited prominent absorption bands at 3446 cm^{-1} and 1635 cm^{-1}, corresponding to hydroxyl (O–H) and carbonyl (C=O) groups, respectively. These peaks expected rise from proteins and other biomolecules secreted by *Bacillus species,* which act as reducing and capping agents during nanoparticle synthesis. Similarly, Petreanu et al. (40) reported that the presence of O–H stretching around 3440 cm^{-1} and C=O stretching near 1630 cm^{-1} indicates the involvement of organic biomolecules such as proteins or polysaccharides in the nanoparticle capping process. These findings support their conclusion that FTIR spectroscopy offers valuable insight into the chemical environment of nanoparticle surfaces and serves as a reliable tool for confirming successful surface functionalization. Peaks at 1100 cm^{-1} and 550 cm^{-1} were attributed to C–O stretching and Ag–O bonding, confirming the presence of silver nanoparticles and indicating their crystalline nature, Comparable spectral characteristics have been reported in related studies (41). The TiO_2 nanoparticles showed similar hydroxyl group peaks at 3444 cm^{-1}, along with a peak at 1628 cm^{-1} associated with bending vibrations of adsorbed water molecules. Characteristic Ti–O stretching and bending vibrations were observed at 1100 cm^{-1} and 643 cm^{-1}, consistent with the anatase phase of TiO_2. These results support earlier findings in the literatures where TiO_2 nanoparticles biosynthesized by bacterial strains exhibited similar vibrational modes. In the Ag-TiO_2 composite, the FTIR spectrum combined features of both individual components, with peaks at 3444 cm^{-1} (O–H), 1746 cm^{-1} (C=O), 1628 cm^{-1} (C=C), and 2927 cm^{-1} (C–H), indicative of organic molecules capping the nanoparticles. The presence of peaks between 500 and 1100 cm^{-1} confirmed Ti–O and Ag–O bonds, verifying successful composite formation. The coexistence of these functional groups indicates synergistic interactions between silver and titanium dioxide within the composite, potentially enhancing catalytic and antibacterial activities. Usman Khan et al. (42) previously reported characteristic FTIR peaks corresponding to hydroxyl (O–H), carbonyl (C=O), and metal-oxygen (Ti–O and Ag–O) bonds, which validated the formation and capping of the nanoparticles. These functional groups are expected derived from biomolecules or capping agents present during the synthesis, contributing significantly to the stability and bioactivity of the nanoparticles. Gupta et al. (43) Similarly reported absorption bands between 500–700 cm^{-1} corresponding to metal–oxygen (M–O) vibrations, specifically Ti–O and Ag–O bonds in titanium dioxide and silver nanoparticles, respectively. These bands confirm the formation of metal oxide frameworks and the successful incorporation of silver within the composite nanoparticles.

FTIR analysis thus confirms the involvement of biomolecules from Bacillus species in nanoparticle synthesis and stabilization. The organic functional groups identified serve a key function in preventing agglomeration and maintaining nanoparticle stability, which is important for their biological applications. (44). Identified characteristic FTIR peaks consistent to hydroxyl (O–H), carbonyl (C=O), and metal–oxygen (M–O) bonds, which indicate the formation and surface modification of nanoparticles. These functional groups pay importantly to nanoparticle stability and promote their interaction with biological systems. Their research highlights the importance of organic compounds and metal–oxygen linkages in nanoparticle coating, which improves their bioactive properties.

- *DLS Analysis*

Dynamic light scattering (DLS) was used to examine the size distribution and average particle size of the biosynthesized silver nanoparticles. For silver nanoparticles (Ag NPs), DLS results showed a Z-average particle size distribution between from 500 to 1000 nm, with peaks at 10nm and 1000 nm, indicating two main size populations. The distribution of TiO_2 NPs was similarly bimodal, with peaks at 500–1000 nm and 10 nm. Ag-TiO_2 composite nanoparticles showed a similar size distribution to Ag NPs, but with lower intensity, and a main particle size around 500–1000 nm, with a smaller peak at 10nm (Figure 4). Dynamic light scattering (DLS) is a widely used method to analyze the particles distribution and hydrodynamic size of nanoparticles (45). It measures light interference from the Brownian motion of particles, correlating their diffusion coefficient with size using the Stokes–Einstein equation. DLS requires low nanoparticle concentrations to minimize multiple scattering effects. The particle size distribution is expressed by the polydispersity index (PDI), ranging from 0 (homogeneous) to 1 (heterogeneous). DLS can also analyze nonspherical particles, like rod-shaped ones, using multiangle techniques. Selim et al. (46) described that Dynamic Light Scattering (DLS) analysis revealed that the Ag-TiO_2 bimetallic nanoparticles (BNPs) had an average hydrodynamic diameter of approximately 79 nm. The DLS technique measures the hydrodynamic radius of nanoparticles, which includes the nanoparticle core as well as the solvent molecules, such as water, that form a surrounding shell. Similarly, Heydari and Ghadam (47) reported, particle size analysis to find out the hydrodynamic diameter of biosynthesized TiO_2 nanoparticles. The normal particle size was found to be approximately 129.68 nm.

- *SEM-EDX Analysis*

Scanning Electron Microscopy (SEM) coupled with Energy-Dispersive X-ray (EDX) spectroscopy was used for analyze the size, morphology, and elemental composition of silver (Ag), titanium dioxide (TiO_2), and Ag-TiO_2 composite nanoparticles synthesized using *Bacillus amyloliquefaciens.* Scanning electron microscopy (SEM), coupled with energy-dispersive X-ray (EDX) analysis, was used to examine the size, morphology, and elemental composition of Ag, TiO_2, and Ag-TiO_2 composite nanoparticles synthesized by *Bacillus amyloliquefaciens*. SEM pictures displayed that both Ag and Ag-TiO_2 composite nanoparticles exhibited a spherical shape with a normal size of around 300 nm, whereas TiO_2

ISSN No:-2456-2165 https://doi.org/10.38124/ijisrt/26aug1001

nanoparticles were larger, measuring around 1 µm (48). The Ag-TiO_2 composite showed a similar size to Ag NPs but with more varied surface morphology (Figure 5). EDX analysis validate the presence of silver and titanium in the samples, with strong silver peaks at 2KeV and 3KeV, and a titanium peak at 4.5 KeV, indicating the decrease of silver ions (Ag^+ to Ag^0) and the existence of TiO_2 in the composite (Figure 6). Scanning electron microscopy (SEM) uses electrons to image nanoparticles with high resolution. Energy dispersive X-ray spectroscopy (SEM-EDX) provides detailed analysis of morphology and elemental composition. SEM-EDX is effective for identifying elements like calcium, silicon, and carbonates, and is widely used for nanoparticle analysis (49, 17).

C. Antimicrobial Activity

The antibacterial properties of biosynthesized Ag and Ag-TiO_2 nanoparticles was assessed against gram-positive bacteria (*Staphylococcus aureus* and *Streptococcus pneumoniae*) and the gram-negative bacterium *Escherichia coli* using the Kirby-Bauer disk diffusion method at concentrations of 1 mg/mL and 5 mg/mL. The outcomes showed that Ag-TiO_2 nanoparticles demonstrated greater antibacterial properties, with zone of inhibition ranging from 13.66 ± 1.52 mm to 22 ± 1.15 mm, compared to Ag nanoparticles, which showed inhibition zones of 10 ± 0.57 mm to 19.33 ± 0.88 mm. The reduced size of Ag-TiO_2 nanoparticles increases their surface area, thereby enhancing efficacy and overall activity. In contrast, TiO_2 nanoparticles showed no antibacterial activity. The positive control, rifampicin at 1 mg/mL, demonstrated inhibitory zones, while Ag, TiO_2, and Ag-TiO_2 nanoparticles showed comparable activity against *Streptococcus pyogenes* Ag (20.66 ± 0.57 mm), TiO_2 (21 ± 1.15 mm), and Ag-TiO_2 (23 ± 0.57 mm), *S. aureus* Ag (21.33 ± 0.32 mm), TiO_2 (20.66 ± 0.57 mm), and Ag-TiO_2 (22 ± 0.57 mm), and *S. pneumoniae* Ag (22.33 ± 0.17 mm), TiO_2 (21.66 ± 0.14 mm), and Ag-TiO_2 (23.33 ± 0.32 mm). Against *E. coli*, Ag nanoparticles showed 21.66 ± 0.14 mm, TiO2 20.66 ± 0.87 mm, and Ag-TiO_2 nanoparticles showed 24 ± 1.15 mm of activity (13). At 5 mg/mL, Ag, TiO_2, and Ag- TiO_2 nanoparticles displayed similar antibacterial properties against *Streptococcus pyogenes* (Ag 22.33 ± 0.32 mm, TiO_2 22.66 ± 1.45 mm, Ag- TiO_2 23.66 ± 0.87 mm), *S. aureus* (Ag 23 ± 0.57 mm, TiO_2 21.33 ± 0.32 mm, Ag- TiO_2 25.33 ± 0.87 mm), and *S. pneumoniae* (Ag 24.33 ± 0.40 mm, TiO_2 20.33 ± 0.32 mm, Ag- TiO_2 25.66 ± 0.32 mm). Against *E. coli*, the inhibition zones measured 27.66 ± 0.76 mm for Ag, 25.66 ± 0.87 mm for TiO_2, and 27.33 ± 0.32 mm for Ag-TiO_2 nanoparticles. At 1 mg/mL, Ag and Ag- TiO_2 nanoparticles showed similar activity against *Streptococcus pyogenes* (Ag 10 ± 0.57 mm, Ag- TiO_2 13.66 ± 1.52 mm). No zones of inhibition were noticed for *S. aureus* and *S. pneumoniae* with both Ag and Ag- TiO_2 nanoparticles. Against *E. coli*, Ag nanoparticles showed no inhibition zone, whereas Ag- TiO_2 nanoparticles demonstrated activity measuring 13.66 ± 0.87 mm. At 5 mg/mL, Ag and Ag- TiO_2 nanoparticles presented comparable activity against *Streptococcus pyogenes* (Ag 22.3 ± 0.80 mm, Ag-TiO2 22 ± 1.15 mm), *S. aureus* (Ag 21.67 ± 1.20 mm, Ag- TiO_2 18.33 ± 0.88 mm), and *S. pneumoniae* (Ag 21 ± 1.73 mm, Ag-TiO2 18 ± 0.58 mm). Against *E. coli*, Ag nanoparticles exhibited 19.33 ± 0.88 mm, and Ag- TiO_2 nanoparticles showed 17.67 ± 0.34 mm of activity (Figure 7). Titanium dioxide (TiO_2) nanoparticles failed to inhibit the growth of the tested pathogens, at any of the evaluated concentrations (1and 5 µg/mL) (Table 1). The increased antibacterial activity of Ag-TiO_2 nanoparticles against *S. aureus* might be because Gram-positive bacteria produce the particles. The antibacterial mechanisms of Ag nanoparticles include cell membrane disruption, ROS generation, and DNA damage, while Ag-TiO_2 NPs also prevent DNA replication by binding to phosphorus in DNA reported by Dua et al. (17) reported the minimum inhibitory concentrations (MIC) of silver nanoparticles (Ag NPs) against the gram-negative bacterium *Escherichia coli* and the gram-positive bacterium *Staphylococcus aureus* as 82.5 µg/mL and 64.5 µg/mL, respectively. The antibacterial assays of Ag NPs are primarily because of their direct interaction with the bacterial cell membrane, resulting in membrane damage and the formation of complexes with cellular components. Additionally, Ag NPs bind to thiol (−SH) groups and induce the generation of reactive oxygen species (ROS) within the cells, leading to oxidative stress and modulation of signal transduction pathways. The antibacterial property of synthesized Ag/TiO_2 nanoparticles (NPs) was documented by Rao et al. (50) against both gram-negative and gram-positive pathogenic bacteria. Additionally, the antifungal potential was assessed using the opportunistic pathogenic yeast *Candida albicans*. The Ag/TiO_2 NPs exhibited the largest zone of inhibition against *Escherichia coli* (24 mm), followed by *C. albicans* (22 mm), methicillin-resistant *Staphylococcus aureus* (20 mm), with the smallest inhibition zone observed against *Pseudomonas aeruginosa* (15 mm) at a concentration of 500 mg/mL. These antimicrobial activity results corroborate previous findings on the efficacy of TiO_2 NPs against drug-resistant bacterial strains. Ibrahim et al. (51) evaluated the antibacterial activity of Ag/TiO_2 nanoparticles using the in vitro well diffusion method. The antimicrobial efficacy of Ag/TiO_2 nanoparticles was evaluated, demonstrating a significant bactericidal effect against several bacterial species. The nanoparticles demonstrated a notable inhibitory zone of 32 mm against the Gram-negative bacterium *Shigella flexneri*. This was larger than the 29 mm zone that was obtained with 30 µg of *streptomycin*. This indicates a potent effect against this specific gram-negative pathogen. Against gram-positive bacteria, the Ag/TiO_2 nanoparticles showed varying degrees of inhibition. They produced a 24 mm zone of inhibition against *S. aureus*, which was lower than the 34 mm zone exhibited by 30 µg of *streptomycin*. However, the nanoparticles demonstrated greater activity against *Bacillus species*, yielding a 38 mm zone of inhibition compared to the 32 mm zone observed with 30 µg of *streptomycin*. These results collectively highlight the broad-spectrum antimicrobial potential of Ag/TiO_2 nanoparticles, confirming their effectiveness against both gram-negative bacteria strain such as *Shigella flexneri* and gram-positive bacteria strain including *Bacillus species*, while demonstrating varied efficacy when compared to standard antibiotics.

D. Antioxidant Assay

➢ *Superoxide (O_2^-) Radical Scavenging Activity*

Ascorbic acid showed the highest superoxide dismutase (SOD) activity, with Ag NPs displaying a decrease in activity as concentration increased, except for a slight rise at 200µg/mL. Ag NPs achieved 50% superoxide scavenging, while ascorbic acid demonstrated 95.51%. TiO_2 NPs also showed a reduction in activity with concentration, with a gradual increase at 100µg/mL, reaching 50% scavenging. Ag-TiO_2 composite NPs exhibited 37.28% scavenging, substantially lower compared to ascorbic acid 95.51% (Figure 8). The DPPH assay confirmed the antioxidant and superoxide scavenging abilities of TiO_2 and Ag-TiO_2 nanoparticles, with DPPH reducing from violet to yellow upon neutralization by antioxidants. As previously reported by Keshari et al. (21) the antioxidant properties of these nanoparticles are largely due to functional groups on their surfaces, especially in Ag NPs, which enhance their ability to neutralize free radicals. The combination of silver and titanium dioxide further boosts this effect, as silver facilitates electron transfer and titanium dioxide provides additional reactive sites. Pudlarz et al. (52) reported that the superoxide dismutase (SOD) activity in colloidal silver nanoparticle solutions reaches its peak at maximum surface coverage, regardless of nanoparticle size, achieving up to 133% activity. Alam et al. (53) found that the presence of nanoparticles enhanced the activity of both enzymes across all tested bacterial strains more effectively than other nanoparticles. This increase is likely linked to the generation of reactive oxygen species (ROS), contributing to their antibacterial effects. Such properties indicate potential applications in cellular defense against oxidative stress and in the mitigation of environmental pollutants.

E. 2,2-Diphenyl-1-Picrylhydrazyl (DPPH) Activity.

The DPPH radical scavenging activity of Ag, TiO_2, and Ag-TiO_2 composite nanoparticles was evaluated at concentrations of 25µg/mL, 50µg/mL, and 75µg/mL, with ascorbic acid as the standard. The results showed significant antioxidant properties for all nanoparticles, with Ag NPs, TiO_2 NPs, and Ag-TiO_2 composite NPs exhibiting high scavenging activity. At 25µg/mL, Ag NPs had 77.8%, TiO_2 NPs 95.9%, and Ag-TiO_2 composite NPs 93.48%. At 50µg/mL, Ag NPs showed 94.9%, TiO_2 NPs 97.35%, and Ag-TiO_2 composite NPs 94.09%. At 75µg/mL, Ag NPs had 96.74%, TiO_2 NPs 97.96%, and Ag-TiO_2 composite NPs 95.92% (Figure 9) (Table 2). Dua et al. (17) demonstrated that silver nanoparticles (AgNPs) display important radical scavenging activity in the DPPH assay, with an IC50 value of 48.96 ± 0.84 µg/mL, compared to the IC50 value of 14.35 ± 0.16 µg/mL for ascorbic acid. The DPPH radical scavenging activity of the synthesized AgNPs was observed to increase in a dose-dependent manner. Nethravathi et al. (54) reported the DPPH free radical's absorption band at 518 nm to estimate the antiradical activity of synthesized nanoparticles. The TiO_2 and Ag/TiO_2 nanoparticles effectively inhibited DPPH free radical activity. The inhibitory concentrations at 50% (IC50) were determined to be 3029 µg/mL for TiO_2 and 3817µg/mL for Ag/TiO_2, respectively. These outcomes show that both types of nanoparticles possess significant antiradical properties, with TiO_2 showing a slightly stronger inhibitory effect on DPPH radicals compared to Ag/TiO_2 under the experimental conditions.

F. Seed Germination

The impact of silver nanoparticles (Ag NPs), titanium dioxide nanoparticles (TiO_2 NPs), and silver-titanium dioxide composite nanoparticles (Ag-TiO_2 Composite NPs) on the seed germination and growth of maize and cucumber was investigated. Higher concentrations of Ag NPs, TiO_2NPs, and Ag-TiO_2 Composite NPs significantly increased the germination rate of maize and cucumber seeds. Notably, Ag NPs markedly enhanced the germination percentages and rates in both maize and cucumber compared to untreated seeds. Specific nanoparticle concentrations yielded optimal germination results. For maize, 2.0 mg/ml Ag NPs led to the highest germination percentage (101.33%) and germination rate (8.53 seeds/day). Cucumber seeds exhibited peak germination percentages (60.57% and 59.47%) and rates (0.53 and 0.64 seeds/day) at 2.0 and 2.5 mg/ml Ag NPs, respectively (Table 3). Treatment with TiO_2 nanoparticles demonstrated concentration-dependent effects on seed germination. At 1.5 mg/mL, TiO_2 NPs promoted the highest germination percentage (60.57%), while the maximum germination rate (7.93 seeds/day) was observed at 2.0 mg/mL. In cucumber, the optimal response differed the highest germination percentage (53.07%) was recorded at 1.0 mg/mL, whereas the peak germination rate (1.97 seeds/day) occurred at 0.5 mg/mL (Table 4). Ag-TiO_2 Composite NPs at 1.0 mg/ml provided the highest germination percentage (95.53%) and rate (4.13 seeds/day) for maize, and for cucumber, 1 mg/ml yielded the highest germination percentage (101.33%) and 1.5 mg/ml resulted in the highest germination rate (2.97 seeds/day) (Table 5). Regarding seedling growth, Ag NPs generally promoted root elongation in both maize and cucumber. For maize, the maximum root length (13.43 cm) was observed at 1.5 mg/ml AgNPs, while for cucumber, the largest mean root length (15.73 cm) occurred at 0.1 mg/ml Ag NPs. Seedling fresh weight for maize increased with higher Ag NP concentrations, with the highest fresh weight (108.13 mg) at 1 mg/ml Ag NPs. Cucumber seedling fresh weight (124.07 mg) was considerably increased by Ag NP treatment at 0.5 mg/ml (Table 6). TiO_2 NPs also influenced seedling growth, with maize exhibiting the highest fresh weight (123.07 mg) at 1 mg/ml and cucumber showing increased fresh weight (94.93 mg) at 0.5 mg/ml (Table 7). Ag-TiO_2 Composite NPs similarly affected seedling growth, with maize demonstrating the highest fresh weight (70.73 mg) at 1 mg/ml, and cucumber showing significant increases in fresh weight (122.33 mg and 122.53 mg) at 1.5 and 2 mg/ml, respectively (Table 8). According to Prazak et al. (55) a seed sample treated with 2.5 mg dm^{-3} of silver nanoparticles (Ag NPs) showed similar results. The seeds were noted at chilling temperatures. The germination capacity of seeds treated with AgNPs at concentrations of 0.25 and 1.25 mg dm^{-3} increased compared to the control seeds. (56). Specifically, the seed germination rates improved by 9.3% and 9.8%, respectively, in the 'Bali' cultivar, and by 10.2% and 11.5% in the 'Delfina' cultivar. Almutairi et al. (22) found that corn seeds exhibited their highest germination rate of 6.50 seeds/day when treated with 1.5 mg/L silver nanoparticles (AgNPs). Watermelon and zucchini seeds responded positively to AgNP treatments, showing significant improvements in germination percentage and rate compared to untreated seeds. Watermelon reached its peak germination percentage of 73.33% and seed germination rate of 1.59 seeds/day at 2 mg/L AgNPs. In zucchini, the maximum seed germination percentages of 86.67% and 90%, along with seed germination rates of 1.68 and 1.66 seeds/day, were achieved at 0.5 mg/L and 2.5 mg/L AgNPs, respectively. Iqbal et al. (57) examined how silver nanoparticles (AgNPs) influence seed germination. For rice, the highest germination percentage reached 90% when treated with 10 mg/100 mL of AgNPs, while increasing the concentration to 15 mg/100 mL resulted in a decrease to 60%. In the case of corn, the optimum germination rate of 85.7% was achieved using 10 mg/100 mL of Ag–TiO_2 nanoparticles, whereas the lowermost seed germination rates were noticed at both 10 mg/100 mL and 15 mg/100 mL AgNPs treatments.

IV. CONCLUSION

This research successfully biosynthesized silver nanoparticles (Ag NPs), titanium dioxide nanoparticles were (TiO_2 NPs), and Ag-TiO_2 composite nanoparticles using *Bacillus amyloliquefaciens*. Characterization was done by UV-visible spectroscopy, X-ray diffraction (XRD), Fourier transform infrared (FTIR) spectroscopy, dynamic light scattering (DLS), and scanning electron microscopy-energy dispersive X-ray spectroscopy (SEM-EDX). The results revealed the crystalline structure, phase purity, and size distribution of the nanoparticles. XRD confirmed the face-centered cubic structure for Ag NPs and anatase phase for TiO_2 NPs, with Ag-TiO_2 composites showing both structures. Functional groups for stabilization and capping were found by FTIR analysis, and a bimodal size distribution with peaks at 500–1000 nm and 10 nm were shown by DLS. SEM-EDX showed Ag NPs at 300 nm, TiO_2 NPs at 1µm, and Ag-TiO_2 composites like Ag NPs. Zones of inhibition at 1 mg/ml and 5 mg/mL ranged from 13 to 18 mm, demonstrating the improved antibacterial activity of Ag-TiO_2 composites over Ag NPs. The SOD assay showed all nanoparticles had superoxide scavenging activity, though less than that ascorbic acid. The DPPH radical scavenging activity of Ag-TiO_2 composites was high, ranging from 93.48% to 95.92% at 25-75µg/mL. In plant growth studies, Ag-TiO_2 composites enhanced root and shoot length in maize, with the highest root length at 2.0mg/mL. TiO_2 NPs positively affected cucumber root and shoot growth at 1.0mg/mL, while Ag NPs also promoted growth to a lesser extent. These results indicate that Ag-TiO_2 composites may have beneficial effects in agriculture by promoting plant growth. Overall, this study highlights the potential of *Bacillus amyloliquefaciens* mediated synthesis of Ag, TiO_2, and Ag-TiO_2 nanoparticles for applications in antibacterial, antioxidant, and agricultural fields. The findings demonstrate that environmentally friendly and sustainable nanoparticles with valuable functional properties can be produced, paving the way for further research and practical applications.

Table 1 Indicates the Antibacterial Activity of Ag, TiO_2 and Ag-TiO_2 Composite NPs. (NZ-no Zone of Inhibition, PC-Positive Control-Rifampicin, NC-Negative Control-Distilled Water).

Bacterial strain, Positive Control (Rifampicin)**, and Negative Control** (Distilled water)	**Ag**		**TiO_2**		**Ag-TiO_2**	
	1mg/ml	**5mg/ml**	**1mg/ml**	**5mg/ml**	**1mg/ml**	**5mg/ml**
Streptococcus pyogenes	10±0.57	22.3±0.80	NZ	NZ	13.66±1.52	22±1.15
Positive Control (Rifampicin)	20.66±0.57	22.33±0.32	21±1.15	22.66±1.45	23±0.57	23.66±0.87
Negative Control (Distilled water)	NZ	NZ	NZ	NZ	NZ	NZ
S. aureus	NZ	21.67±1.20	NZ	NZ	NZ	18.33±0.88
Positive Control (Rifampicin)	21.33±0.32	23±0.57	20.66±0.57	21.33±0.32	22±0.57	25.33±0.87
Negative Control (Distilled water)	NZ	NZ	NZ	NZ	NZ	NZ
S. pneumonia	NZ	21±1.73	NZ	NZ	NZ	18±0.58
Positive Control (Rifampicin)	22.33±0.17	24.33±0.40	21.66±10.14	20.33±0.32	23.33±0.32	25.66±0.32
Negative Control (Distilled water)	NZ	NZ	NZ	NZ	NZ	NZ
E. coli	NZ	19.33±0.88	NZ	NZ	13.66±0.87	17.67±0.34
Positive Control (Rifampicin)	21.66±10.14	27.66±0.76	20.66±0.87	25.66±0.87	24±1.15	27.33±0.32
Negative Control (Distilled water)	NZ	NZ	NZ	NZ	NZ	NZ

Table 2 The DPPH Radical Scavenging Activity of Ag, TiO_2, and Ag-TiO_2 Composite Nanoparticles

Nanoparticles	**Ascorbic acid**	**25µg/mL**	**50µg/mL**	**75µg/mL**
Ag NPs	95.52%	93.48%	94.09%	95.92%
TiO_2 NPs	95.52%	95.91%	97.35%	97.96%
Ag-TiO_2 composite NPs	95.52%	93.48%	94.09%	95.92%

ISSN No:-2456-2165 https://doi.org/10.38124/ijisrt/26aug1001

Table 3 Influence of Ag NPs, Concentrations on Germination Percentages, Germination Rates and Mean Germination Times for Maize, and Cucumber Plants. M = Mean, SD =Standard Deviations, GP =Germination Percentage, GR = Germination Rate and MGT = Mean Germination Time, mg = Milligram, ml = Milliliter, cm = Centimeter, %= Percentage.

Ag NPs concentrations			Control	0.05 mg/ml	0.1 mg/ml	0.5 mg/ml	1 mg/ml	1.5 mg/ml	2.0 mg/ml	2.5 mg/ml
Maize	GP%	M	81.33	85.6	94.9	96.03	96.8	99.67	101.33	99.33
		SD	0.58	0.7	0.62	0.60	0.52	0.58	1.15	0.58
	GR (seed/day)	M	5.33	6.47	7.53	7.73	8.43	7.93	8.53	7.48
		SD	0.58	0.55	0.47	0.55	0.49	0.38	0.47	0.37
	MGT (day)	M	2.33	2.47	2.67	2.97	2.63	2.83	2.17	1.47
		SD	0.58	0.55	0.58	0.32	0.55	0.17	0.05	0.38
Cucumber	GP%	M	40.33	40.73	41.83	44.23	50.57	54.9	60.57	59.47
		SD	0.58	0.55	0.46	0.12	0.64	0.53	0.53	0.64
	GR (seed/day)	M	0.73	1.27	1.67	2.67	2.77	3.57	3.63	2.83
		SD	1.01	0.05	0.40	0.40	0.35	0.45	0.48	0.12
	MGT (day)	M	1.47	1.67	2.97	3.23	2.67	2.63	1.47	1.17
		SD	0.38	0.40	0.32	0.05	0.58	0.55	0.38	0.05

Table 4 Influence of TiO_2 NPs Concentrations on Germination Percentages, Germination Rates and Mean Germination Times for Maize, and Cucumber Plants. M = Mean, SD =Standard Deviations, GP =Germination Percentage, GR = Germination Rate and MGT = Mean Germination Time, mg = Milligram, ml = Milliliter, cm = Centimeter, % = Percentage.

TiO_2 NPs concentrations			Control	0.05 mg/ml	0.1 mg/ml	0.5 mg/ml	1 mg/ml	1.5 mg/ml	2mg/ml	2.5 mg/ml
Maize	GP%	M	40.43	50.33	54.43	52.57	54.43	60.57	56.83	50.43
		SD	0.67	0.58	0.49	0.52	0.49	0.39	0.64	0.67
	GR (seed/day)	M	4.57	5.13	5.33	5.47	6.47	7.63	7.93	7.57
		SD	0.46	0.25	0.58	0.52	0.55	0.40	0.45	0.52
	MGT (day)	M	0.73	1.33	1.37	1.07	1.03	0.23	0.17	0.13
		SD	1.01	0.47	0.55	0.06	0.06	0.06	0.06	0.06
Cucumber	GP%	M	40.13	42.53	45.03	48.57	53.07	51.07	48.57	45.87
		SD	0.06	0.50	0.60	0.73	0.34	0.54	0.52	0.47
	GR (seed/day)	M	0.47	0.67	0.47	1.97	1.37	1.03	0.97	0.17
		SD	0.52	0.46	0.52	0.15	0.55	0.06	0.40	0.12
	MGT (day)	M	1.47	2.03	2.73	3.97	3.13	2.63	3.07	2.97
		SD	0.38	0.23	0.47	0.17	0.25	0.48	0.26	0.12

Table 5 Influence of Ag-TiO_2 Composite NPs Concentrations on Germination Percentages, Germination Rates and Mean Germination Times for Maize, and Cucumber Plants. M = Mean, SD =Standard Deviations, GP =Germination Percentage, GR = Germination Rate and MGT = Mean Germination Time, mg = Milligram, ml = Milliliter, cm = Centimeter, %= Percentage.

Ag-TiO_2 Composite NPs concentrations			Control	0.05 mg/ml	0.1 mg/ml	0.5 mg/ml	1 mg/ml	1.5 mg/ml	2 mg/ml	2.5 mg/ml
Maize	GP%	M	82.53	84.67	88.07	90.37	95.53	92.77	90.27	87.57
		SD	0.47	0.59	0.26	0.05	0.47	0.47	0.09	0.45
	GR (seed/day)	M	2.37	2.97	3.17	3.87	4.13	3.67	3.23	2.63
		SD	0.46	0.57	0.60	0.25	0.25	0.58	0.12	0.40
	MGT (day)	M	2.83	3.13	3.53	3.00	2.77	2.97	2.03	1.47
		SD	0.52	0.25	0.47	0.26	0.31	0.12	0.23	0.38
Cucumber	GP%	M	84.67	96.03	96.8	99.67	101.33	99.33	94.9	85.6
		SD	0.59	0.60	0.52	0.58	1.15	0.58	0.62	0.7
	GR (seed/day)	M	2.17	2.37	2.47	3.53	2.67	2.97	2.63	1.97
		SD	0.05	0.46	0.55	0.47	0.58	0.32	0.55	0.15
	MGT (day)	M	1.47	2.67	3.83	2.77	3.63	2.83	2.67	2.37
		SD	0.38	0.40	0.29	0.35	0.42	0.12	0.40	0.46

ISSN No:-2456-2165 https://doi.org/10.38124/ijisrt/26aug1001

Table 6 Influence of AgNPs, TiO_2 NPs and Ag-TiO_2 Composite NPs Concentrations on Root Lengths, Seedling Fresh and Dry Weights of Maize, and Cucumber Plants. M = Mean, SD = Standard Deviations, RL = Root Length, FW =Seedling Fresh Weight, DW = Seedling Dry Weight, mg = Milligram, ml = Milliliter, cm = Centimeter.

Ag NPs concentrations			**Control**	**0.05 mg/ml**	**0.1 mg/ml**	**0.5 mg/ml**	**1 mg/ml**	**1.5 mg/ml**	**2 mg/ml**	**2.5 mg/ml**
Maize	**RL (cm)**	**M**	9.07	9.27	10.63	10.67	13.33	13.43	12.13	11.17
		SD	0.62	0.09	0.47	0.47	0.47	0.59	0.52	0.17
	FW (mg)	**M**	93.6	98.07	101.47	104.13	108.13	112.13	114.73	110.87
		SD	0.43	0.47	0.74	0.41	0.38	0.41	0.47	0.47
	DW (mg)	**M**	11.63	11.17	13.6	16.67	20.57	23.57	19.63	17.07
		SD	0.46	0.17	0.43	0.41	0.59	0.59	0.40	0.37
Cucumber	**RL (cm)**	**M**	9.73	10.73	15.73	11.47	12.53	13.73	11.13	11.8
		SD	0.34	0.50	0.62	0.45	0.42	0.62	0.52	0.57
	FW (mg)	**M**	94.93	98.00	100.67	124.07	101.87	102.27	114.07	119.93
		SD	0.52	0.43	0.52	0.47	0.47	0.50	0.19	0.38
	DW (mg)	**M**	9.67	11.07	14.67	28.13	17.07	20.27	25.33	22.13
		SD	0.38	0.34	3.35	0.25	1.09	0.50	0.38	0.25

Table 7 Influence of TiO_2 NPs Concentrations on Root Lengths, Seedling Fresh and Dry Weights of Maize, and Cucumber Plants. M = Mean, SD = Standard Deviations, RL = Root Length, FW =Seedling Fresh Weight, DW = Seedling Dry Weight, mg = Milligram, ml = Milliliter, cm = Centimeter.

TiO_2 NPs concentrations			**Control**	**0.05 mg/ml**	**0.1 mg/ml**	**0.5 mg/ml**	**1 mg/ml**	**1.5 mg/ml**	**2 mg/ml**	**2.5 mg/ml**
Maize	**RL (cm)**	**M**	4.47	5.47	6.93	9.27	11.67	13.93	15.87	11.67
		SD	0.19	0.38	0.62	0.50	0.52	0.34	0.38	0.47
	FW (mg)	**M**	88.33	98.73	102.87	105.57	123.07	118.13	101.67	100.33
		SD	0.47	0.47	0.53	0.12	0.81	0.57	0.47	0.09
	DW (mg)	**M**	10.93	13.73	15.87	16.87	17.93	20.53	19.67	17.87
		SD	0.19	0.34	0.68	0.25	0.53	0.47	0.38	0.53
Cucumber	**RL (cm)**	**M**	8.67	9.13	9.47	9.93	12.87	10.83	11.03	9.73
		SD	0.47	0.17	0.38	0.05	0.53	0.17	0.61	0.62
	FW (mg)	**M**	79.73	84.27	89.13	94.93	87.17	83.43	79.17	71.73
		SD	0.62	0.47	0.53	0.68	0.69	0.21	0.40	0.34
	DW (mg)	**M**	29.87	31.87	38.73	41.87	52.73	48.87	45.73	40.93
		SD	0.52	0.52	0.62	0.38	0.34	0.52	0.50	0.34

Table 8 Influence of Ag-TiO_2 Composite NPs Concentrations on Root Lengths, Seedling Fresh and Dry Weights of Maize, and Cucumber Plants. M = Mean, SD = Standard Deviations, RL = Root Length, FW =Seedling Fresh Weight, DW = Seedling Dry Weight, mg = Milligram, ml = Millilitre, cm = Centimetre.

Ag-TiO2 Composite NPs concentrations			**Control**	**0.05 mg/ml**	**0.1 mg/ml**	**0.5 mg/ml**	**1 mg/ml**	**1.5 mg/ml**	**2 mg/ml**	**2.5 mg/ml**
Maize	**RL (cm)**	**M**	12.27	15.93	17.87	19.93	24.33	24.13	20.87	17.83
		SD	0.09	0.34	0.52	0.62	0.38	0.38	0.68	0.68
	FW (mg)	**M**	40.83	54.73	58.77	64.00	65.67	70.73	67.67	64.23
		SD	0.68	0.62	0.66	1.23	0.47	0.58	0.47	0.45
	DW (mg)	**M**	12.03	19.53	24.17	28.73	35.63	25.97	23.07	18.67
		SD	0.48	0.47	0.48	0.54	0.54	0.48	0.56	0.47
Cucumber	**RL (cm)**	**M**	11.33	13.47	15.73	17.07	25.77	21.77	18.93	13.53
		SD	0.47	0.45	0.26	0.69	0.45	0.60	0.54	0.40
	FW (mg)	**M**	94.93	98.87	104.53	107.67	117.77	122.33	122.53	114.67
		SD	0.52	0.48	0.48	0.33	0.39	0.47	4.78	0.45
	DW (mg)	**M**	9.67	11.43	16.47	23.73	33.83	26.03	21.33	19.63
		SD	0.38	0.05	0.05	0.48	0.54	0.45	0.47	0.40

International Journal of Innovative Science and Research Technology
https://doi.org/10.38124/ijisrt/26aug1001

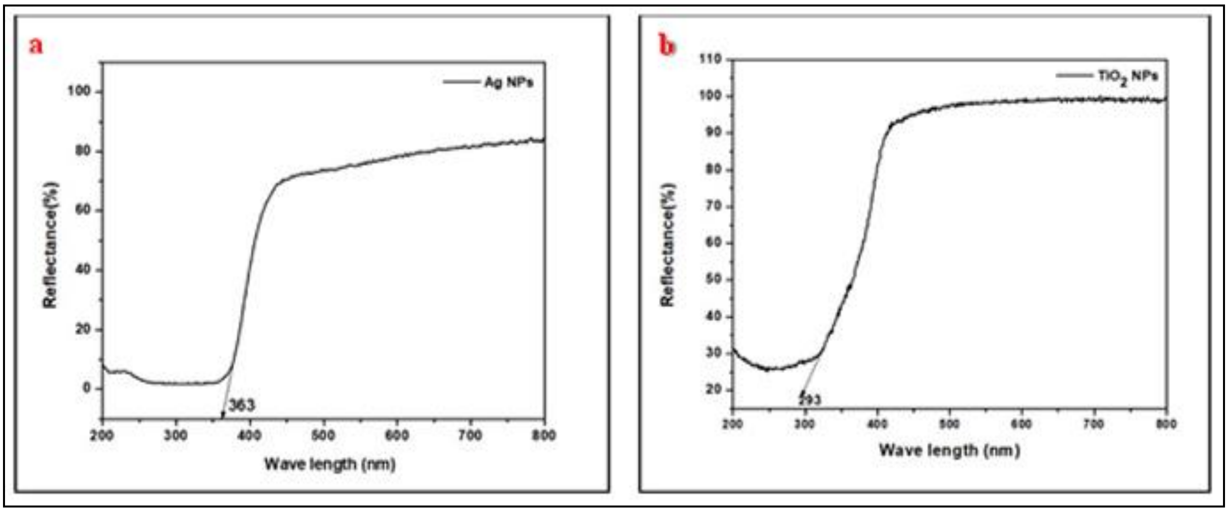

Fig 1 UV-Visible Spectral Analysis of Biosynthesized (a). Ag NPs, (b). TiO_2 NPs and (C) Ag-TiO_2NPs Composite.

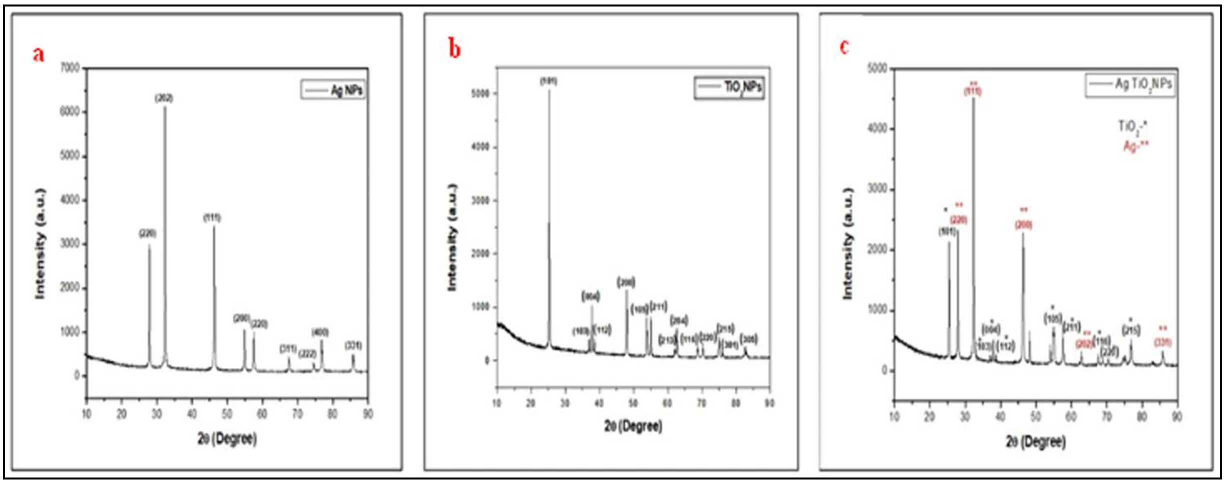

Fig 2 (a): XRD Pattern of Biosynthesized Ag NPs (b): XRD Pattern of Biosynthesized TiO_2 NPs (c): XRD Pattern of Biosynthesized Ag-TiO_2 NPs

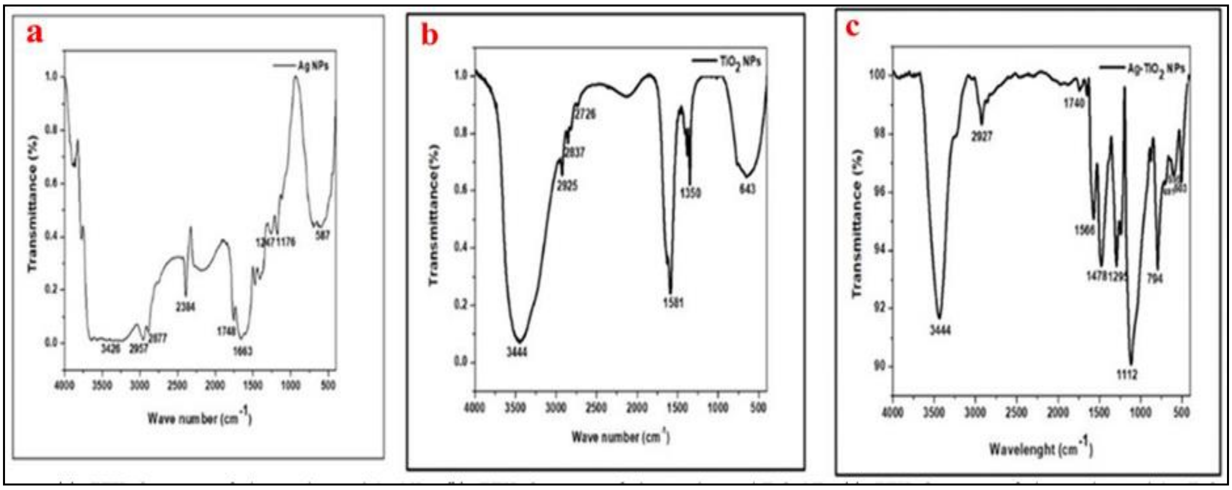

Fig 3 (a): FTIR Spectrum of Biosynthesized Ag NPs, (b): FTIR Spectrum of Biosynthesized TiO_2 NPs (c): FTIR Spectrum of Biosynthesized Ag-TiO_2 NPs

International Journal of Innovative Science and Research Technology
ISSN No:-2456-2165
https://doi.org/10.38124/ijisrt/26aug1001

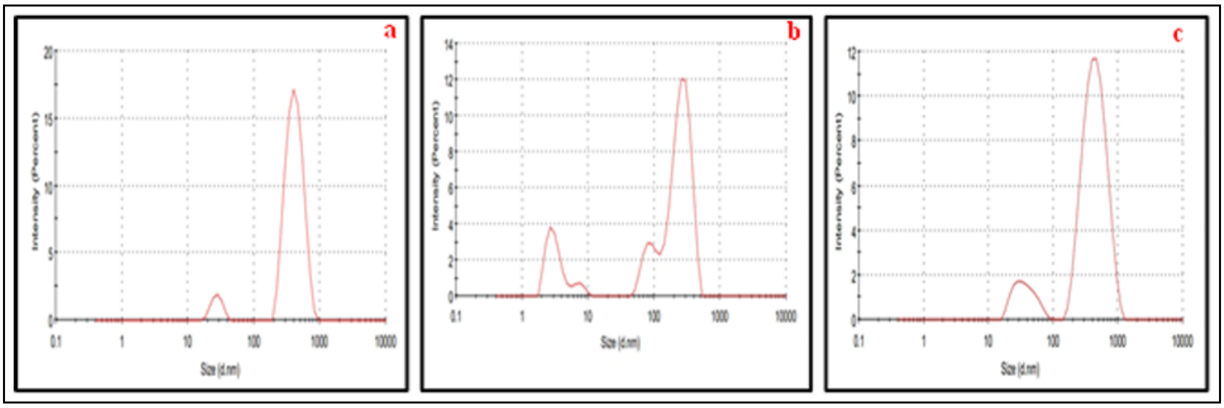

Fig 4 (a): DLS Analysis of Biosynthesized Ag NPs (b): DLS Analysis of Biosynthesized TiO_2 NPs (c): DLS Analysis of Biosynthesized Ag-TiO_2 NPs

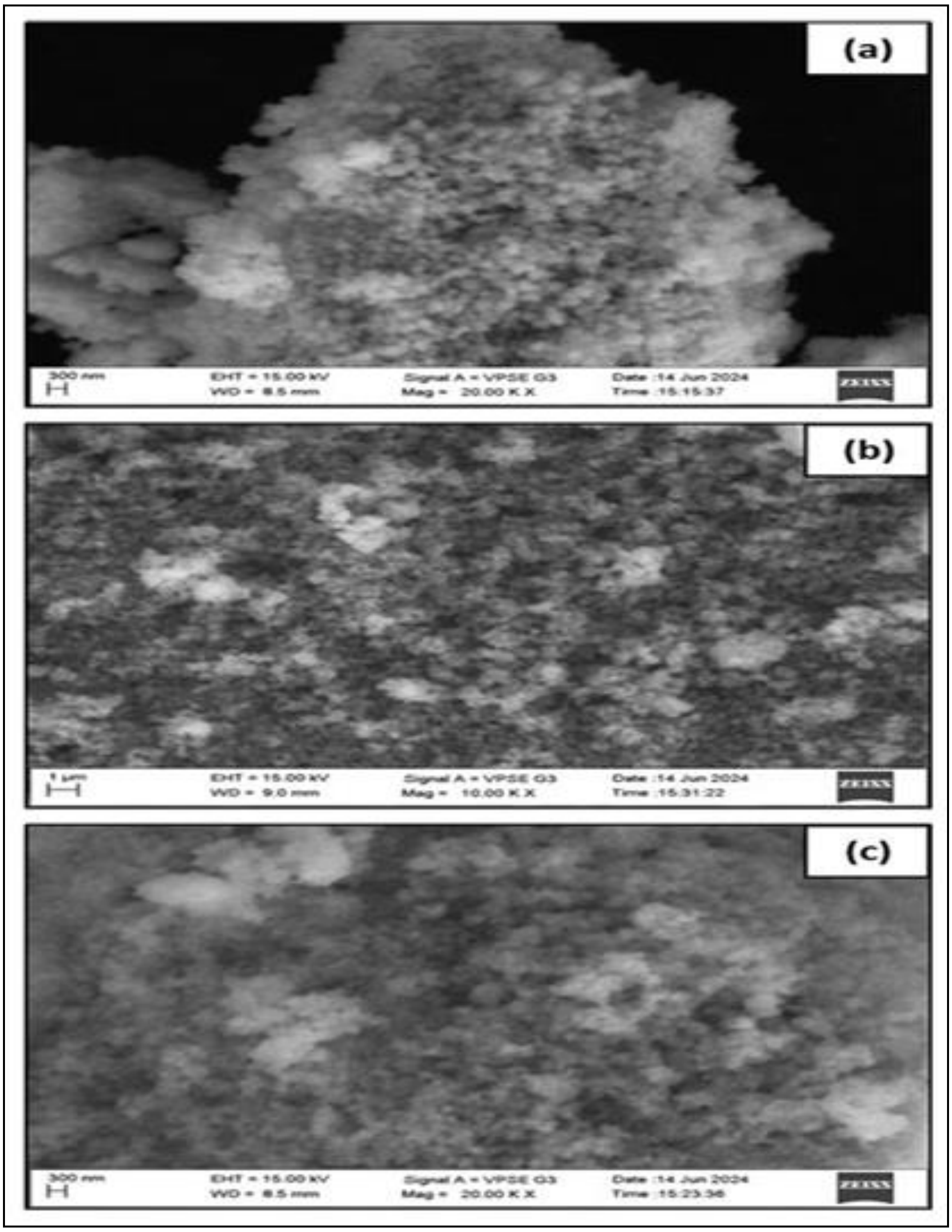

Fig 5 (a): Scanning electron microscope (SEM) images displays the crystalline shape of (a). Ag NPs, (b). TiO_2 NPs and (c) Ag-TiO_2 NPs composite with different magnifications. The features appear as clustered particles or aggregates, with a resolution of 300 nm. (b): At a different magnification of 10,000 times, this image reveals a more uniform texture over a larger field, emphasizing the arrangement of particles at 1 µm scale. The distribution of particles is less distinct compared to (a), appearing more integrated. (c): Similar to (a) in magnification, this image shows structures with a 300 nm resolution.

ISSN No:-2456-2165 https://doi.org/10.38124/ijisrt/26aug1001

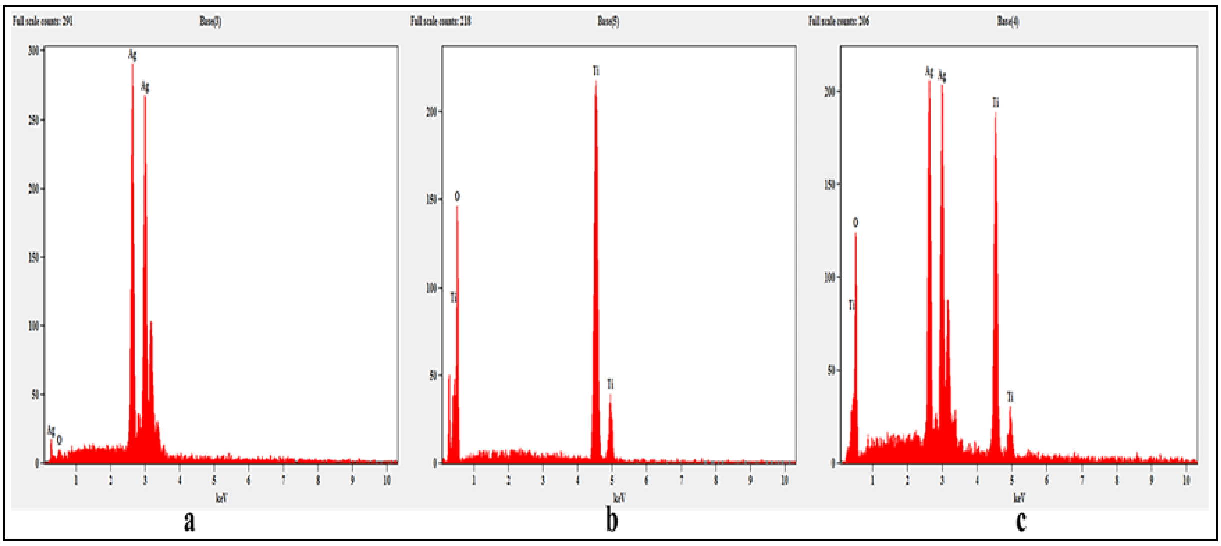

Fig 6 EDX Analysis of Biosynthesized a. Ag NPs, b. TiO_2 NPs c. Ag- TiO_2 Composite NPs

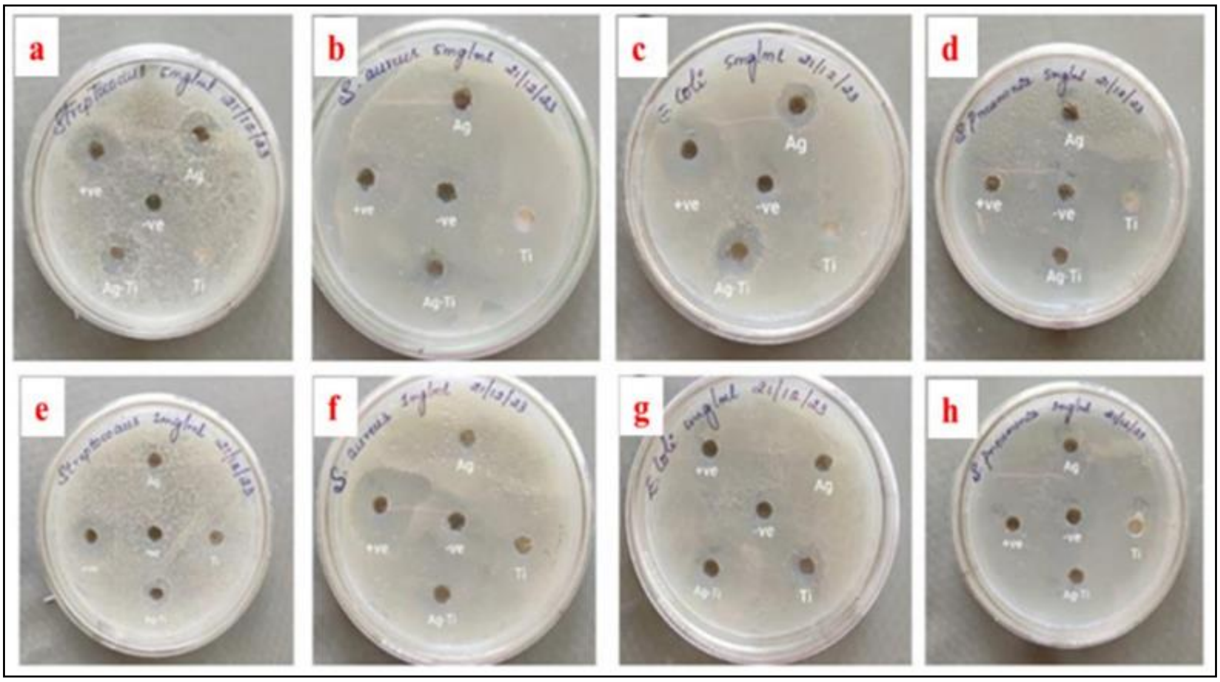

Fig 7 Indicates the Antibacterial Activity of Ag, TiO_2 and Ag-TiO_2 Composite NPs a. (*Streptococcus pyogenes*), b. (*S. aureus*), c (*E. coli*), d. (*S. pneumonia*) at 5mg/ml Concentration. e. (*Streptococcus pyogenes*), f. (*S. aureus*), g. (*E. coli*), h. (*S. pneumonia*) at 1mg/ml Concentration (Positive Control=Rifampicin, Negative Control=Distilled Water)

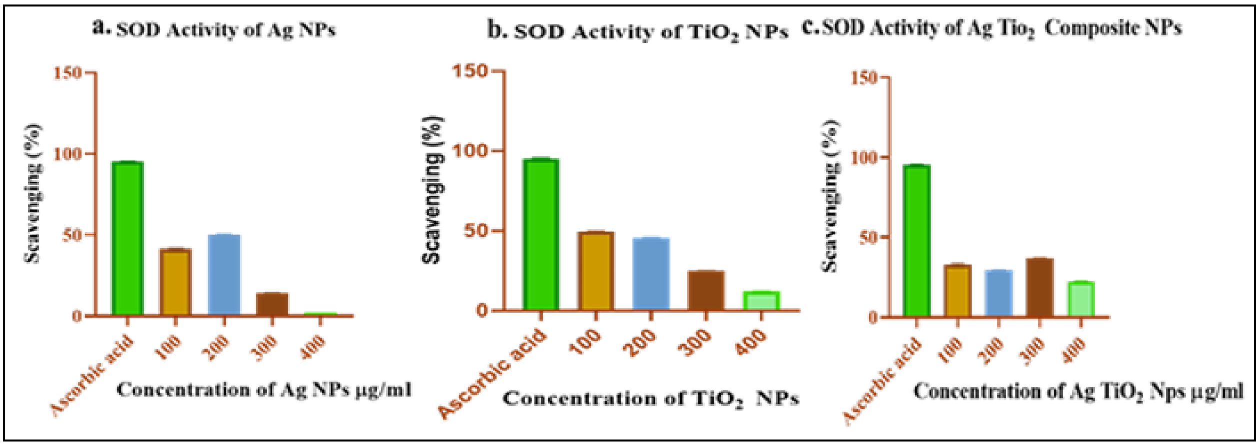

Fig 8 SOD Activity of (a). Ag NPs, (b). TiO_2 NPs and (C) Ag-TiO_2 Composite NPs.

ISSN No:-2456-2165 https://doi.org/10.38124/ijisrt/26aug1001

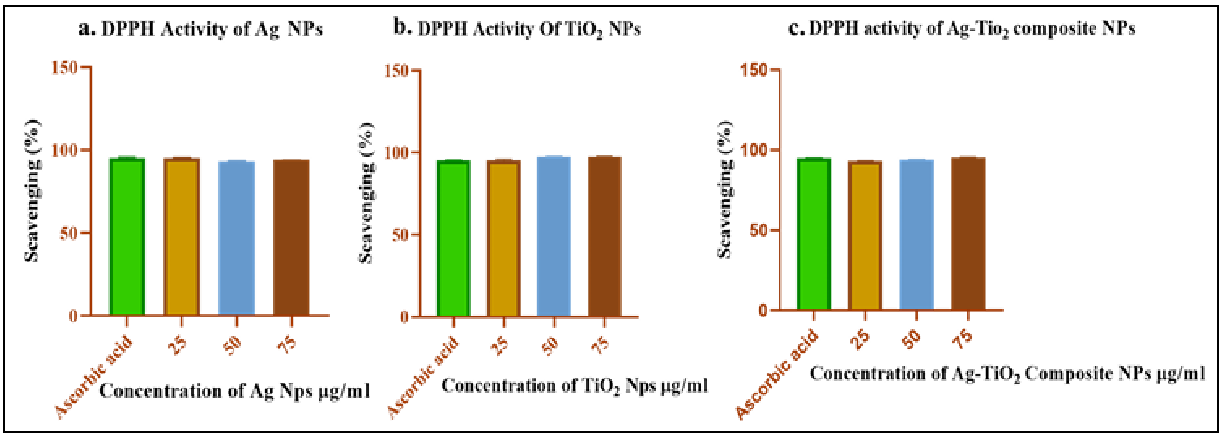

Fig 9 DPPH Free Radical Scavenging Activity of (a). Ag NPs, (b). TiO_2 NPs and (C) Ag-TiO_2 Composite NPs.

ACKNOWLEDGMENT

We are grateful to the Department of Studies and Research in Biotechnology, Jnanasiri Campus, Tumkur University, and Centre for Research and Innovations, Adichunchanagiri university, Mandya, Karnataka for providing the necessary facilities.

- *Conflict of Interest*

The authors declare no conflict of interest.

- *Author Contributions*

SA, GM and SC designed research. SA, and GM, performed the experiments. SA and SC analyze the experimental data. SA, GM and SC drafting the research manuscript. SA and SC editing the research manuscript. All the authors have read and approved the research manuscript.

- *Data Availability Statement*

The data that support the findings of this study are available from the corresponding author upon reasonable request.

REFERENCES

[1]. WoldemariamYohannes K, Wan Z, Yu Q, Li H, Wei X, Liu Y, Wang J, Sun B. Prebiotic, probiotic, antimicrobial, and functional food applications of *Bacillus amyloliquefaciens*. J Agric Food Chem. 2020;68:14709–14727. https://doi.org/10.1021/acs.jafc.0c06396.

[2]. Algburi A, Alazzawi SA, Al-Ezzy AIA, Weeks R, Chistyakov V, Chikindas ML. Potential probiotics *Bacillus subtilis* KATMIRA1933 and *Bacillus amyloliquefaciens* B-1895 co-aggregate with clinical isolates of *Proteus mirabilis* and prevent biofilm formation. Probiotics Antimicrob Proteins. 2020;12:1471–1483. https://doi.org/10.1007/s12602-020-09631-0.

[3]. Du H, Yao W, Kulyar MFEA, Ding Y, Zhu H, Pan H, Li K, Bhutta ZA, Liu S, Li J. Effects of *Bacillus amyloliquefaciens* TL106 isolated from Tibetan pigs on probiotic potential and intestinal microbes in weaned piglets. Microbiol Spectr. 2022;10:e01205-21. https://doi.org/10.1128/spectrum.01205-21.

[4]. Ngalimat MS, Yahaya RSR, Baharudin MMAA, Yaminudin SM, Karim M, Ahmad SA, Sabri S. A review on the biotechnological applications of the operational group *Bacillus amyloliquefaciens*. Microorganisms. 2021;9:614. https://doi.org/10.3390/microorganisms9030614.

[5]. Rani N, Singh P, Kumar S, Kumar P, Bhankar V, Kumar K. Plant-mediated synthesis of nanoparticles and their applications: a review. Mater Res Bull. 2023;163:112233. https://doi.org/10.1016/j.materresbull.2023.112233.

[6]. Hano C, Abbasi BH. Plant-based green synthesis of nanoparticles: production, characterization and applications. Biomolecules. 2022;12:31. https://doi.org/10.3390/biom12010031.

[7]. Singh NA, Narang J, Garg D, Jain V, Payasi D, Suleman S, Swami RK. Nanoparticles synthesis via microorganisms and their prospective applications in agriculture. Plant Nano Biol. 2023;5:100047. https://doi.org/10.1016/j.plana.2023.100047

[8]. Wang Z, Chen C, Liu H, Hrynshpan D, Savitskaya T, Chen J, Chen J. Enhanced denitrification performance of *Alcaligenes* sp. TB by Pd stimulating to produce membrane adaptation mechanism coupled with nanoscale zero-valent iron. Sci Total Environ. 2020;708:135063. https://doi.org/10.1016/j.scitotenv.2019.135063.

[9]. Rathore C, Yadav VK, Amari A, Meena A, Chinedu Egbosiuba T, Verma RK, Mahdhi N, Choudhary N, Sahoo DK, Chundawat RS, Patel A. Synthesis and characterization of titanium dioxide nanoparticles from *Bacillus subtilis* MTCC 8322 and its application for the removal of methylene blue and orange G dyes under UV light and visible light. Front Bioeng Biotechnol. 2024;11:1323249. https://doi.org/10.3389/fbioe.2023.1323249.

[10]. Fouda A, Hassan SED, Saied E, Azab MS. An eco-friendly approach to textile and tannery wastewater treatment using maghemite nanoparticles (γ-Fe_2O_3-NPs) fabricated by *Penicillium expansum* strain (Kw). J Environ Chem Eng. 2021;9:104693. https://doi.org/10.1016/j.jece.2020.104693.

[11]. Fouda A, Eid AM, Abdelkareem A, Said HA, El-Belely EF, Alkhalifah DHM, Alshallash KS, Hassan SED. Phyco-synthesized zinc oxide nanoparticles using

ISSN No:-2456-2165 https://doi.org/10.38124/ijisrt/26aug1001

marine macroalgae, *Ulva fasciata* Delile, characterization, antibacterial activity, photocatalysis, and tanning wastewater treatment. Catalysts. 2022;12:756. https://doi.org/10.3390/catal12070756.

[12]. Al Malki JS, Hussien NA, Akkad LM, Al Thurmani SO, Al Motiri AE. Green synthesis of silver and titanium oxide nanoparticles using tea and eggshell wastes, their characterization, and biocompatibility evaluation. Sustainability. 2023;15:11858. https://doi.org/10.3390/su151511858.

[13]. Al-Asbahi MG, Al-Ofiry BA, Saad FA, Alnehia A, Al-Gunaid MQ. Silver nanoparticles biosynthesis using mixture of *Lactobacillus* sp. and *Bacillus* sp. growth and their antibacterial activity. Sci Rep. 2024;14:10224. https://doi.org/10.1038/s41598-024-59936-1.

[14]. Mondal AH, Yadav D, Mitra S, Mukhopadhyay K. Biosynthesis of silver nanoparticles using culture supernatant of *Shewanella* sp. ARY1 and their antibacterial activity. Int J Nanomedicine. 2020;15:8295–8310. https://doi.org/10.2147/IJN.S274535.

[15]. Shanthi S, Jayaseelan BD, Velusamy P, Vijayakumar S, Chih CT, Vaseeharan B. Biosynthesis of silver nanoparticles using a probiotic *Bacillus licheniformis* Dahb1 and their antibiofilm activity and toxicity effects in *Ceriodaphnia cornuta*. Microb Pathog. 2016;93:70–77. https://doi.org/10.1016/j.micpath.2016.01.014.

[16]. Mohmed AA, Saad E, Fouda A, Elgamal MS, Salem SS. Extracellular biosynthesis of silver nanoparticles using *Aspergillus* sp. and evaluation of their antibacterial and cytotoxicity. J Appl Life Sci Int. 2017;11:1–12. https://doi.org/10.9734/JALSI/2017/33491.

[17]. Dua TK, Giri S, Nandi G, Sahu R, Shaw TK, Paul P. Green synthesis of silver nanoparticles using *Eupatorium adenophorum* leaf extract: characterizations, antioxidant, antibacterial and photocatalytic activities. Chem Pap. 2023;77:2947–2956. https://doi.org/10.1007/s11696-023-02676-9.

[18]. Wei W, Yu D, Huang Q. Preparation of Ag/TiO_2 nanocomposites with controlled crystallization and properties as a multifunctional material for SERS and photocatalytic applications. Spectrochim Acta Part A Mol Biomol Spectrosc. 2020;243:118793. https://doi.org/10.1016/j.saa.2020.118793.

[19]. Yadav VK, Amari A, Wanale SG, Osman H, Fulekar MH. Synthesis of floral-shaped nanosilica from coal fly ash and its application for the remediation of heavy metals from fly ash aqueous solutions. Sustainability. 2023;15:2612. https://doi.org/10.3390/su15032612.

[20]. Mohd Yusof H, Abdul Rahman NA, Mohamad R, Zaidan UH, Samsudin AA. Biosynthesis of zinc oxide nanoparticles by cell-biomass and supernatant of *Lactobacillus plantarum* TA4 and its antibacterial and biocompatibility properties. Sci Rep. 2020;10:19996. https://doi.org/10.1038/s41598-020-76402-w.

[21]. Keshari AK, Srivastava R, Singh P, Yadav VB, Nath G. Antioxidant and antibacterial activity of silver nanoparticles synthesized by *Cestrum nocturnum*. J Ayurveda Integr Med. 2020;11:37–44. https://doi.org/10.1016/j.jaim.2017.11.003.

[22]. Almutairi Z. Effect of silver nanoparticles on seed germination of crop plants. J Adv Agric. 2015;4:4295. https://doi.org/10.24297/jaa.v4i1.4295.

[23]. Xin X, Zhao F, Rho JY, Goodrich SL, Sumerlin BS, He Z. Use of polymeric nanoparticles to improve seed germination and plant growth under copper stress. Sci Total Environ. 2020;745:141055. https://doi.org/10.1016/j.scitotenv.2020.141055.

[24]. International Seed Testing Association. International rules for seed testing: seed health testing methods is the supplement to chapter 7 international rules for seed testing; edition 2013; catalogued separately. 2013.

[25]. Oshone K, Gebeyehu S, Tesfaye K. Assessment of common bean (*Phaseolus vulgaris* L.) seed quality produced under different cropping systems by smallholder farmers in Eastern Ethiopia. Afr J Food Agric Nutr Dev. 2014;14:8566.

[26]. Ellis RH, Roberts EH. The quantification of ageing and survival in orthodox seeds. Seed Sci Technol. 1981;9(2).

[27]. Jimoh AA, Akpeji BH, Azeez SO, Ayipo YO, Abdulsalam ZA, Adebayo ZF, Ajao AT, Zakariyah AT, Elemike EE. Biosynthesis of Ag and TiO_2 nanoparticles and the evaluation of their antibacterial activities. Inorg Chem Commun. 2022;141:109503. https://doi.org/10.1016/j.inoche.2022.109503.

[28]. Rahman MS, Chakraborty A, Kibria A, Hossain MJ. Effects of silver nanoparticles on seed germination and growth performance of pea (*Pisum sativum*). Plant Nano Biol. 2023;5:100042. https://doi.org/10.1016/j.plana.2023.100042.

[29]. Khan S, Zahoor M, Khan RS, Ikram M, Islam NU. The impact of silver nanoparticles on the growth of plants: the agriculture applications. Heliyon. 2023;9:e16928. https://doi.org/10.1016/j.heliyon.2023.e16928.

[30]. Fouad H, Hongjie L, Yanmei D, Baoting Y, El-Shakh A, Abbas G, Jianchu M. Synthesis and characterization of silver nanoparticles using *Bacillus amyloliquefaciens* and *Bacillus subtilis* to control filarial vector *Culex pipiens pallens* and its antimicrobial activity. Artif Cells Nanomed Biotechnol. 2017;45:1369–1378. https://doi.org/10.1080/21691401.2016.1241793.

[31]. Hieu HN, Trang DTH, Hien VTT, Nghia NV, Lam NT, Nguyen TMD. Microorganism-mediated green synthesis of silver nanoparticles using *Aspergillus niger* and *Bacillus megaterium*. Dig J Nanomater Biostruct. 2022;17:359–367. https://doi.org/10.15251/DJNB.2022.171.359.

[32]. Quevedo AC, Guggenheim E, Briffa SM, Adams J, Lofts S, Kwak M, Lee TG, Johnston C, Wagner S, Holbrook TR, Hachenberger YU. UV-Vis spectroscopic characterization of nanomaterials in aqueous media. JoVE. 2021;176:e61764. https://doi.org/10.3791/61764.

[33]. Titus D, Samuel EJJ, Roopan SM. Nanoparticle characterization techniques. In: Green synthesis, characterization and applications of nanoparticles.

Elsevier; 2019. p. 303–319. https://doi.org/10.1016/B978-0-08-102579-6.00012-5.
[34]. Uthiravel V, Narayanamurthi K, Raja V, Anandhabasker S, Kuppusamy K. Green synthesis and characterization of TiO_2 and Ag-doped TiO_2 nanoparticles for photocatalytic and antimicrobial applications. Inorg Chem Commun. 2024;170:113327. https://doi.org/10.1016/j.inoche.2024.113327.
[35]. Rathore R, Choudhary KK, Kaurav N. The structural and optical properties of zinc-oxide nanomaterials synthesized via thermal decomposition method. J Phys Conf Ser. 2023;2603:012003. https://doi.org/10.1088/1742-6596/2603/1/012003.
[36]. Awad MA, Alanazi MM, Hendi AA, Virk P, Alrowaily AW, Bahlool T, Alhakami FS, Aouaini F, Ibrahim EM. Potential role of 'green' synthesized titanium dioxide nanoparticles in photocatalytic applications. Crystals. 2022;12:1639. https://doi.org/10.3390/cryst12111639.
[37]. Abd Elkodous M, El-Khawaga AM, Abouelela MM, Abdel Maksoud MIA. Cocatalyst loaded Al-$SrTiO_3$ cubes for Congo red dye photo-degradation under wide range of light. Sci Rep. 2023;13:6331. https://doi.org/10.1038/s41598-023-33249-1.
[38]. Herrero YR, Camas KL, Ullah A. Characterization of biobased materials. In: Advanced applications of biobased materials. Elsevier; 2023. p. 111–143. https://doi.org/10.1016/B978-0-323-91677-6.00005-2.
[39]. Carrapico A, Martins MR, Caldeira AT, Mirao J, Dias L. Biosynthesis of metal and metal oxide nanoparticles using microbial cultures: mechanisms, antimicrobial activity and applications to cultural heritage. Microorganisms. 2023;11:378. https://doi.org/10.3390/microorganisms11020378.
[40]. Petreanu I, Niculescu VC, Enache S, Iacob C, Teodorescu M. Structural characterization of silica and amino-silica nanoparticles by Fourier transform infrared (FTIR) and Raman spectroscopy. Anal Lett. 2023;56:390–403. https://doi.org/10.1080/00032719.2022.2083144.
[41]. Jain AS, Pawar PS, Sarkar A, Junnuthula V, Dyawanapelly S. Bionanofactories for green synthesis of silver nanoparticles: toward antimicrobial applications. Int J Mol Sci. 2021;22:11993. https://doi.org/10.3390/ijms222111993.
[42]. Usman Khan M, Rehman W, Bibi S, Alanazi MM, Alanazi AS, Rasheed L, Khan S, Tariq Gillani SU, Tauqeer A. Synthesis, characterization, and antimicrobial and nematicidal activities of chitosan-based silver-doped titanium dioxide. ACS Omega. 2023;8:19341–19350. https://doi.org/10.1021/acsomega.3c00068.
[43]. Gupta J, Arya S, Verma S, Singh A, Sharma A, Singh B, Sharma R. Performance of template-assisted electrodeposited Copper/Cobalt bilayered nanowires as an efficient glucose and uric acid sensor. Mater Chem Phys. 2019;238:121969. https://doi.org/10.1016/j.matchemphys.2019.121969.
[44]. Ahmed I, Mir FA, Banday JA. Synthesis of metal and metal oxide nanoparticles using plant extracts characterization and applications. BioNanoScience. 2023;13:1541–1557. https://doi.org/10.3390/jfb13040274.
[45]. Filippov SK, Khusnutdinov R, Murmiliuk A, Inam W, Zakharova LY, Zhang H, Khutoryanskiy VV. Dynamic light scattering and transmission electron microscopy in drug delivery: a roadmap for correct characterization of nanoparticles and interpretation of results. Mater Horiz. 2023;10:5354–5370. https://doi.org/10.1039/D3MH00717K.
[46]. Selim S, Badr BM, Moustafa MH, Saied E, Elkady FM, Salama A, Aloufi AS, Algamdi NA, Alzahofi NN, Abada E, Alshammari MS. Green biosynthesis of bimetallic silver titanium dioxide nanoparticles using *Pluchea indica* with their anticancer, antimicrobial, and antioxidant activities. Sci Rep. 2025;15:26735. https://doi.org/10.1038/s41598-025-10349-8.
[47]. Heydari Z, Ghadam P. Biosynthesis of titanium dioxide nanoparticles by the aqueous extract of *Juglans regia* green husk. Mater Proc. 2023;14:43. https://doi.org/10.3390/IOCN2023-14482.
[48]. Joshi SM, De Britto S, Jogaiah S, Ito SI. Mycogenic selenium nanoparticles as potential new generation broad spectrum antifungal molecules. Biomolecules. 2019;9:419. https://doi.org/10.3390/biom9090419.
[49]. Kaliva M, Vamvakaki M. Nanomaterials characterization. In: Polymer science and nanotechnology. Elsevier; 2020. p. 401–433. https://doi.org/10.1016/B978-0-12-816806-6.00017-0.
[50]. Rao TN, Babji P, Ahmad N, Khan RA, Hassan I, Shahzad SA, Husain FM. Green synthesis and structural classification of *Acacia nilotica* mediated-silver doped titanium oxide (Ag/TiO_2) spherical nanoparticles: assessment of its antimicrobial and anticancer activity. Saudi J Biol Sci. 2019;26:1385–1391. https://doi.org/10.1016/j.sjbs.2019.09.005.
[51]. Ibrahim S, Ali J, Rajasekar S, Chakravarthy NS, Varsha, Singh MS, Kumar V, Saruchi. Synthesis, characterization of Ag/TiO_2 nanocomposite: its anticancer and anti-bacterial activities. Glob Nest J. 2022;24:262–266. https://doi.org/10.30955/gnj.004255.
[52]. Pudlarz AM, Ranoszek-Soliwoda K, Czechowska E, Tomaszewska E, Celichowski G, Grobelny J, Szemraj J. A study of the activity of recombinant Mn-superoxide dismutase in the presence of gold and silver nanoparticles. Appl Biochem Biotechnol. 2019;187:1551–1568. https://doi.org/10.1007/s12010-018-2896-y.
[53]. Alam H, Khatoon N, Khan MA, Husain SA, Saravanan M, Sardar M. Synthesis of selenium nanoparticles using probiotic bacteria *Lactobacillus acidophilus* and their enhanced antimicrobial activity against resistant bacteria. J Cluster Sci. 2020;31:1003–1011. https://doi.org/10.1007/s10876-019-01705-6.
[54]. Nethravathi PC, Nagaraju G, Suresh D. TiO_2 and Ag-TiO_2 nanomaterials for enhanced photocatalytic and antioxidant activity: green synthesis using *Cucumis melo* juice. Mater Today Proc. 2022;49:841–848. https://doi.org/10.1016/j.matpr.2021.05.670.
[55]. Prazak R, Swiecilo A, Krzepilko A, Michalek S, Arczewska M. Impact of Ag nanoparticles on seed

germination and seedling growth of green beans in normal and chill temperatures. Agriculture. 2020;10:312. https://doi.org/10.3390/agriculture10080312.

[56]. Haleke Besaye B, Galgaye GG. Impact of common bean (*Phaseolus vulgaris* L.) genotypes on seed yield, and seed quality at different locations of Eastern Ethiopia. Cogent Food Agric. 2022;8:2115674. https://doi.org/10.1080/23311932.2022.2115674.

[57]. Iqbal T, Irfan F, Afsheen S, Zafar M, Naeem S, Raza A. Synthesis and characterization of Ag–TiO_2 nano-composites to study their effect on seed germination. Appl Nanosci. 2021;11:2043–2057. https://doi.org/10.1007/s13204-021-01912-6.